Computational and biological approaches in repurposing ribavirin for lung cancer treatment: Unveiling antitumorigenic strategies

Keshav Raj Paudel, Manisha Singh, Gabriele De Rubis, Popat Kumbhar, Samir Mehndiratta, Sofia Kokkinis, Tammam El-Sherkawi, Gaurav Gupta, Sachin Kumar Singh, Md Zubbair Malik, Yousuf Mohammed, Brian G. Oliver, John Disouza, Vandana Patravale, Philip Michael Hansbro, Kamal Dua

PII: S0024-3205(24)00449-1

DOI: https://doi.org/10.1016/j.lfs.2024.122859

Reference: LFS 122859

To appear in: *Life Sciences*

Received date: 7 January 2024

Revised date: 11 March 2024

Accepted date: 18 June 2024

Please cite this article as: K.R. Paudel, M. Singh, G. De Rubis, et al., Computational and biological approaches in repurposing ribavirin for lung cancer treatment: Unveiling antitumorigenic strategies, *Life Sciences* (2024), https://doi.org/10.1016/j.lfs.2024.122859

Computational and Biological Approaches in Repurposing Ribavirin for Lung Cancer Treatment: Unveiling Antitumorigenic Strategies

Keshav Raj Paudel[1,#], Manisha Singh[2,#], Gabriele De Rubis[3,4], Popat Kumbhar[5], Samir Mehndiratta[3,4], Sofia Kokkinis[3,4], Tammam El-Sherkawi[3,4], Gaurav Gupta[6,7,8], Sachin Kumar Singh[4,9], Md. Zubbair Malik[10], Yousuf Mohammed[11], Brian G. Oliver[12,13], John Disouza[5], Vandana Patravale[14], Philip Michael Hansbro[1,*] Kamal Dua[3,4,**]

[1]Centre of Inflammation, Centenary Institute and University of Technology Sydney, Faculty of Science, School of Life Sciences, Sydney, NSW 2007, Australia

[2]Department of Pharmaceutical Chemistry, JSS College of Pharmacy, JSS Academy of Higher Education and Research, Sri Shivarathreeshwara Nagara, Mysuru 570015, India

[3]Discipline of Pharmacy, Graduate School of Health, University of Technology Sydney, Sydney, NSW 2007, Australia

[4]Faculty of Health, Australian Research Centre in Complementary and Integrative Medicine, University of Technology Sydney, Ultimo, NSW 2007, Australia

[5]Department of Pharmaceutics, Tatyasaheb Kore College of Pharmacy, Warananagar, Tal: Panhala, Dist: Kolhapur, Maharashtra, 416113, India

[6]Center for Global Health Research, Saveetha Medical College, Saveetha Institute of Medical and Technical Sciences, Saveetha University, Chennai, Tamil Nadu 602105, India

[7]School of Pharmacy, Graphic Era Hill University, Dehradun 248007, India

[8]School of Pharmacy, Suresh Gyan Vihar University, Jagatpura 302017, Mahal Road, Jaipur, India

[9]School of Pharmaceutical Sciences, Lovely Professional University, Jalandhar-Delhi GT Road, Phagwara 144411, Punjab, India

[10]Department of Genetics and Bioinformatics, Dasman Diabetes Institute, Dasman, Kuwait city 15462, Kuwait

[11]Frazer Institute, Faculty of Medicine, The University of Queensland, Brisbane, QLD 4102, Australia

[12]Woolcock Institute of Medical Research, University of Sydney, Sydney, New South Wales, Australia

[13]School of Life Sciences, University of Technology Sydney, Ultimo, NSW 2007, Australia

[14]Department of Pharmaceutical Sciences and Technology, Institute of Chemical Technology, Nathalal Parekh Marg, Matunga, Mumbai, 400019, Maharashtra, India

*Corresponding author:

Prof Philip M Hansbro,

Centre of Inflammation,

Centenary Institute and University of Technology Sydney,

Faculty of Science,

School of Life Sciences, Sydney, NSW 2007, Australia

E-mail: philip.hansbro@uts.edu.au

Tel: +61 2 9565 6248

**Corresponding author:

Dr Kamal Dua,

Discipline of Pharmacy,

Graduate School of Health,

University of Technology Sydney,

Sydney, NSW 2007, Australia

E-mail: Kamal.Dua@uts.edu.au

Tel: +61 2 9514 7387

# First author with equal contribution

Acknowledgments

KD is supported by a project grant from the Rebecca L Cooper Medical Research Foundation and the Maridulu Budyari Gumal Sydney Partnership for Health, Education, Research and Enterprise (SPHERE) RSEOH CAG Seed grant, fellowship and extension grant and the UTS Faculty of Health MCR/ECR Mentorship Support Grant. KRPs is supported by a joint fellowship from Prevent Cancer Foundation and International Association for the Study of Lung Cancer (IASLC) USA. KD, GDR, and KRP are supported by the Maridulu Budyari Gumal Sydney Partnership for Health, Education, Research and Enterprise (SPHERE) RSEOH CAG and Triple I Seed and extension grants, Triple I Skills Advancement Grants 2023 and the UTS Faculty of Health Industry Partnership Grant. GDR and KD are also supported by the UTS 2023 Key Technology Partner (KTP) grants.

ABSTRACT

Lung cancer is among leading causes of death worldwide. The five-year survival rate of this disease is extremely low (17.8%), mainly due to difficult early diagnosis and to the limited efficacy of currently available chemotherapeutics. This underlines the necessity to develop innovative therapies for lung cancer. In this context, drug repurposing represents a viable approach, as it reduces the turnaround time of drug development removing costs associated to safety testing of new molecular entities. Ribavirin, an antiviral molecule used to treat hepatitis C virus infections, is particularly promising as repurposed drug for cancer treatment, having shown therapeutic activity against glioblastoma, acute myeloid leukemia, and nasopharyngeal carcinoma. In the present study, we thoroughly investigated the *in vitro* anticancer activity of ribavirin against A549 human lung adenocarcinoma cells. From a functional standpoint, ribavirin significantly inhibits cancer hallmarks such as cell proliferation, migration, and colony formation. Mechanistically, ribavirin downregulates the expression of numerous proteins and genes regulating cell migration, proliferation, apoptosis, and cancer angiogenesis. The anticancer potential of ribavirin was further investigated *in silico* through gene ontology pathway enrichment and protein-protein interaction networks, identifying five putative molecular interactors of ribavirin (Erb-B2 Receptor Tyrosine Kinase 4 (Erb-B4); KRAS; Intercellular Adhesion Molecule 1 (ICAM-1); amphiregulin (AREG); and neuregulin-1 (NRG1)). These interactions were characterized *via* molecular docking and molecular dynamic simulations. The results of this study highlight the potential of ribavirin as a repurposed chemotherapy against lung cancer, warranting further studies to ascertain the *in vivo* anticancer activity of this molecule.

Keywords: lung cancer; drug repurposing; ribavirin; computational biology; docking; molecular dynamics

1. Introduction

Lung cancer is a global health burden and is among the leading causes of death worldwide, representing about 20% of all cancer-related deaths [1, 2]. In 2020, lung cancer has claimed nearly 1.7 million lives throughout the world [3]. Despite the availability of numerous treatment strategies such as chemotherapy, radiotherapy, surgical resection, and immunotherapy, the life expectancy of lung cancer patients is still extremely low, with a five-year survival rate of 17.8% [4, 5]. This underlines the necessity to develop innovative (example: nanotechnology, advance drug delivery system, chronotherapy, microRNA inhibitors, metallic nanoparticles), more effective treatment strategies to tackle the burden of lung cancer [6-13].

In the context of developing novel treatments, the inhibition of cancer hallmarks such as abnormal cell proliferation, cell migration and invasion, neo-vascularization, dysregulation of the cell cycle, apoptosis, and epigenetic changes represent key treatment strategies [14-18]. However, cancer cell metastasis represents a significant challenge as it not only promotes the spreading of cancer but also reduces treatment efficacy [19]. Furthermore, it is a well-established fact that cancer cells develop resistance to anticancer drugs through various mechanisms, contributing to cancer progression [20]. All these factors, combined with the elevated cost of developing new drugs, make anticancer treatment a challenge for many suffering from cancers, including lung cancer [21, 22].

Recently, there has been a paradigm shift in the efforts of researchers toward the repurposing of existing drugs, consisting in identifying new therapeutic applications for existing clinically approved drugs. Also known as drug reprofiling or repositioning, examples of drug repurposing became more evident during and post-COVID era, where scientist repurposed various antiviral drugs for the treatment of COVID. Additionally, many other anti-viral drugs have also been repurposed for various infections and other diseases. Some examples include favipiravir and sofosbuvir, which display promising efficacy against Ebola virus and Zika virus infections [19, 23].

Similarly, to address the challenges posed by cancer and its treatment, drug repurposing has emerged as a compelling strategy to find effective treatments [24]. Drug repurposing not only considerably reduces costs and time investment in the new drug research and development, but it also reaps the benefits from the plethora of information available on drugs already tested in

human clinical trials [25]. Resistance to the existing anticancer drugs has further fuelled the interest of scientists working in the field of oncology towards drug repurposing.

Additionally, various anti-depressant [26] and anti-viral agents have been explored for their anti-cancer properties [27]. Drugs like acyclovir [27] and azido thymidine [28, 29] (Figure 1), for example, have been investigated for their potential in the treatment of breast cancer and various other cancer types [19]. Nelfinavir, a protease inhibitor for HIV (Figure 1), has anticancer effects *via* inhibiting the Akt signalling pathway and by inducing endoplasmic reticulum stress [30]. Ribavirin, a well-known anti-viral agent used to treat hepatitis C virus (HCV) infection (Figure 1), is a guanosine analogue and RNA synthesis inhibitor that has shown effectiveness in treating COVID-19 [31], glioblastoma, acute myeloid leukemia (AML), and nasopharyngeal carcinoma (NPC) [32].

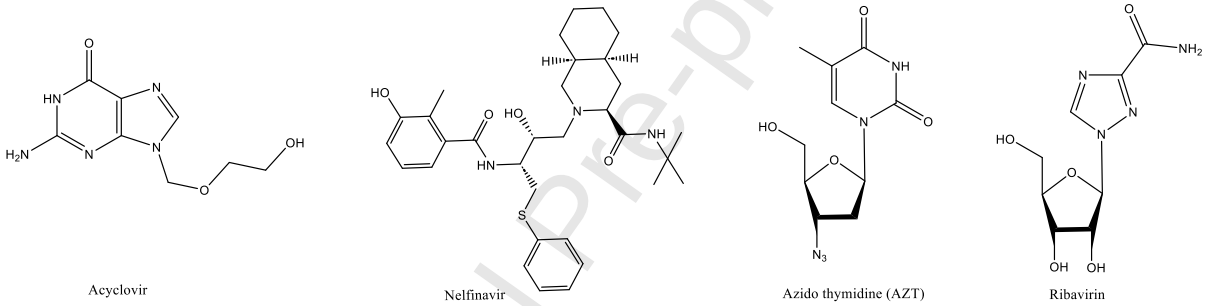

Figure 1: Examples of some of the repurposed drugs that are under investigation for the treatment of cancer.

Ribavirin has been reported to display its anticancer effects mechanistically *via* modulating pathways involving proteins such as Enhancer Of Zeste 2 Polycomb Repressive Complex 2 Subunit (EZH2), Snail, eukaryotic translation initiation factor 4E (eIF4E), mammalian target of rapamycin (mTOR), cyclin D1, and inosine-5′-monophosphate dehydrogenase (IMPDH) for treatment of nasopharyngeal carcinoma, breast cancer, thyroid cancer, glioblastoma, and others [33-35]. Ribavirin has also been reported to target and reduce the activity of matrix metalloproteinase-3 (MMP-3) and matrix metalloproteinase-9 (MMP-9), two fundamental mediators of cancer cell migration and invasion [36]. In a recent study from our team, we demonstrated that ribavirin downregulates the expression of the interleukins (ILs) IL-6 and IL-8, two cytokines that play a major role in cancer progression, in A549 human lung adenocarcinoma cells, providing further proof of the potential of ribavirin as anticancer drug [37].

Furthermore, drug repurposing has been supported by the computational revolution, which has allowed the exploration of available data across different platforms to streamline the process of drug repurposing [38]. Furthermore, various approaches, such as knowledge-based drug repurposing, target-based drug repurposing, pathway-based drug repurposing, gene expression profiling, network analysis, and protein-ligand docking studies, have significantly contributed to the exponential development of this innovative field [39-43].

In the present study, we have thoroughly investigated the *in vitro* anticancer potential of ribavirin against A549 cells. Our results indicate that ribavirin, at concentrations of 25 µM, significantly inhibits cancer hallmarks such as cell proliferation, cell migration, and colony formation. Mechanistically, this effect was exerted by decreasing the expression of several proteins associated with proliferation (ErbB3, ErbB4, enolase 3 and others), migration/invasion/metastasis (angiopoietin-like 4, thrombospondin-1,mesothelin, and others), and angiogenesis (VE-cadherin and human chorionic gonadothropin), as demonstrated *via* proteome profiler protein array. At the mRNA level, ribavirin also decreased the expression of the oncogenes Kirsten rat sarcoma viral oncogene homolog (KRAS) and v-raf murine sarcoma viral oncogene homolog B1 (BRAF). These results were supported by *in silico* computational analysis, which was performed through gene ontology pathway enrichment and the investigation of protein interaction networks. From these studies, five putative interactors of ribavirin were identified: Erb-B2 Receptor Tyrosine Kinase 4 (Erb-B4); KRAS; Intercellular Adhesion Molecule 1 (ICAM-1); amphiregulin (AREG); and neuregulin-1 (NRG1). The interaction of these five hits was further investigated with molecular docking studies, as well as through molecular dynamics simulation of the interaction of ribavirin with ERBB4 and KRAS.

In summary, the present report elucidates the promising anticancer potential of ribavirin in A549 lung cancer cells, and the underlying mechanism through which ribavirin exerts this activity, further identifying five putative interactors of this molecule. The results of the present study provide foundational information for further investigation towards the repurposing of ribavirin as an anticancer agent in the treatment of lung cancer, to be used either as monotherapy or as combination therapy with commonly used chemotherapeutics. In order to achieve this goal, *in vitro* confirmation of the identified putative interactions should be performed, as well as a thorough *in vivo* investigation of the anticancer potential of ribavirin.

2. Materials and Methods

2.1. Cell culture and treatment with Ribavirin

Human lung adenocarcinoma cells (A549) and human bronchial epithelial cells (BEAS-2B), both sourced from ATCC, USA, were a kind gift from Woolcock Institute of Medical Research, Sydney, Australia. The cells were cultured in Dulbecco's Modified Eagle Medium (DMEM) low-glucose (Sigma-Merck, Australia). The culture medium was supplemented with 1% v/v penicillin/streptomycin solution (Sigma-Merck, Australia) and 5% v/v FBS (Sigma-Merck, Australia). The cells were kept at 37 °C, in a humidified environment with 5% CO_2. Ribavirin (Sigma-Merck, Australia) was dissolved at a stock concentration of 80 mM in sterile phosphate-buffered saline (PBS, Sigma-Merck, Australia), and diluted to the final concentration with complete DMEM.

2.2. Cell proliferation assay – MTT

In order to assess the anti-proliferative effect of ribavirin on A549 cells, and its effect on BEAS-2B cell viability, an MTT assay was conducted as reported previously [44-46]. Briefly, 5000 cells/well were seeded in a volume of 200 µL complete DMEM in a 96-well plate and left to attach overnight. The next day, the cells were treated with concentrations of ribavirin ranging between 2.5 and 200 µM for 72 hours. After treatment, a concentration of 250 µg/mL MTT ((3-(4,5-dimethylthiazol-2-yl)-2,5-diphenyl tetrazolium bromide, Sigma-Merck, Australia) was added to each well, and the cells were incubated for 4 hours at 37°C. After the incubation, the supernatant was aspirated and the formazan crystals obtained dissolved in 100 µL dimethyl sulfoxide (DMSO, Sigm-Merck, Australia). The absorbance of the wells was read at a wavelength of 570 nm in a plate reader (TECAN Infinite M1000, Tecan Trading AG, Switzerland).

2.3. Cell migration assay – wound healing assay

With the aim of investigating the effect of ribavirin on the migratory capacity of A549 cells, a wound healing assay was performed as described previously [47-49]. A549 cells were seeded at a density of 100,000 cells/well in a volume of 2 mL complete DMEM, in 6-well plates. The cells were then grown until confluency at 37°C. A scratch was then created at the center of

each well with a sterile 200 µL pipette tip. The wells were then washed with sterile PBS five times to remove the detached cells, and treated with 0 or 25 µM ribavirin for up to 72 hours. The distance between the two edges of the scratches was then imaged with a light microscope, at a magnification of 10X, upon 0, 24, 48, and 72 hours of ribavirin treatment. The distance between the edges was then measured using the ImageJ software (version 1.53c, Bethesda, MD, USA). The wound closure of the ribavirin-treated groups was indicated as percentage compared to the control untreated group.

2.4. Cell migration assay – transwell chamber assay

Transwell chamber assay to quantify A549 migration was done as described previously with slight modifications [50]. As A549 cell doubling time is approximately 22 hours, we allowed the A549 cells treated with or without 25µM of ribavirin to migrate from the upper compartment of transwell to the lower compartment for 16 hours (less than the cells' doubling time) to validate the anti-migratory activity. The non-migrated cells on the upper surface of the membrane were cleaned using cotton swabs. The cells migrated to the lower surface of the membrane were fixed in 10% formalin, stained with hematoxylin and eosin, and cover-slipped to take microscopic images at 40X magnification.

2.5. Colony formation assay – crystal violet staining

To assess the efficacy of ribavirin in inhibiting the colony formation capacity of A549 cells, a crystal violet assay was performed as reported previously [44]. A549 cells were seeded at low density (500 cells/well) in 6-well plates and left to adhere overnight. The next day, cells were treated with 0 or 25 µM ribavirin for 72 hours. After treatment, the cells were left to grow in complete DMEM until visible colonies were observed in the control (untreated) group (about 2 weeks). During this time, the culture media was replaced every 72 hours. After colony development, the cells were washed 3 times with PBS and fixed with 4% formaldehyde for 30 minutes. This was followed by three washes with PBS and by staining with 0.4% w/v crystal violet (Sigma-Merck, Australia). Finally, the cells were washed three times with PBS and photographed. The number of colonies formed were counted manually.

2.6. Gene expression analysis – real-time qPCR

To assess the effect of ribavirin on the mRNA expression levels of the genes *KRAS* and *BRAF*, real-time qPCR was performed as reported in a previous study [51, 52].

2.6.1. Cell treatment and harvesting

A549 cells were seeded at a density of 100,000 cells/well in 6-well plates and left to attach overnight. The next day, the cells were treated with 0 or 25 µM ribavirin for 72 hours. After treatment, the cells were washed 3 times with ice-cold PBS, followed by lysis and harvesting with 500 µL TRIreagent (Sigma-Merck, Australia). The samples were frozen at -80°C until use.

2.6.2. RNA extraction

Immediately before extracting the RNA, the samples were thawed on ice and vortexed for 45 seconds to maximize cell rupture. Successively, 125 µL chloroform (Sigma-Merck, Australia) were added to each sample. The samples were pulse-vortexed and incubated for 15 minutes at room temperature. After incubation, the samples were centrifuged at 12,000 g for 15 minutes, at 3°C, to separate the aqueous phase and the organic phase. The aqueous layer was then carefully aspirated and transferred into fresh tubes. Successfully, the RNA was precipitated by adding 250 µL of ice-cold isopropanol (Sigma-Merck, Australia) to the aqueous phase. The tubes were pulse-vortexed, incubated at room temperature for 10 minutes, and centrifuged at 12,000 g, for 10 minutes, at a temperature of 3°C. The supernatant was then removed, and the RNA pellets washed twice with 1 mL of 75% ethanol (Sigma-Merck, Australia). After each wash, the tubes were centrifuged at 8,000 g for 5 minutes at a temperature of 3°C. The ethanol was then carefully aspirated, and the samples were left to dry on ice until complete evaporation of the remaining ethanol. The dry pellets were then dissolved in 20 µL nuclease-free water (Sigma-Merck, Australia). The concentration and purity of the obtained RNA samples were assessed using a NanoDrop spectrophotometer (Thermo Fisher Scientific, Waltham, MA, USA). Only samples with a 260/280 ratio > 1.8, a 260/230 ratio > 2.00, and a concentration > 150 ng/µL were used in the successive steps.

2.7.3. Reverse Transcription

The RNA samples were first diluted to a concentration of 100 ng/µL with nuclease-free water. 8 µL of RNA solution, corresponding to 800 ng RNA, were then transferred to a 0.5 µL PCR tube. The samples were subjected to treatment with DNAse I (Sigma-Merck, Australia) and then reverse transcribed using, in the reaction mixture: 1X M-MLV reaction buffer (Sigma-Merck, Australia); 0.5 µg/µL random hexamer primers (ThermoFisher Scientific, Australia); 10 mM dNTPs (ThermoFisher Scientific, Australia); 100 mM dithiothreitol (DTT, ThermoFisher Scientific, Australia). The reverse transcription was performed in an Eppendorf Flexlid Mastercycler Nexus thermal cycler (Hamburg, Germany) with the following program: denaturation (65 °C, 10 min); annealing (25°C, 10 min), reverse transcription (37°C, 50 min), and reverse transcriptase inactivation (70°C, 15 min). The samples were diluted to a final volume of 100 µL (corresponding to approximately 8 ng/µL cDNA) before performing the qPCR.

2.8.4. Real-time qPCR

The real-time qPCR was performed using 2 µL of each cDNA, corresponding to 16 ng cDNA. The reaction was performed using the iTaq Universal SYBR green mix (BioRad, USA), following the manufacturer's instructions. Gene-specific forward and reverse primers (Sigma-merch, Australia) were used at a final concentration of 0.5 µM each, in a final reaction volume of 10.5 µL per sample. The qPCR protocol was run in a CFX96 thermal cycler (BioRad, USA), using the following protocol: initial denaturation (95°C for 30 s for one cycle); 95°C for 15 s and 60°C for 30 s (alternated, for 50 cycles). The human glyceraldehyde-3-phosphate dehydrogenase (*GAPDH*) gene was used as an internal normalization control. The sequences of the human gene primers used were as follows:

Gene name	**FW sequence**	**RV sequence**
KRAS	GCCTGCTGAAAATGACTG	TCCTGTAGGAATCCTCTATTG
BRAF	ATATCTGGAGGCCTATGAAG	CTGAAAGAGATGAAGGTAGC
GAPDH	TCGGAGTCAACGGATTTG	CAACAATATCCACTTTACCAGAG

2.7. Protein expression analysis – oncology protein array

To assess the effect of ribavirin on A549 cancer cells proliferation, migration/invasion, metastasis, and angiogenesis, a Proteome Profiler Human XL Oncology Array kit (R&D Systems, USA) was used, as reported previously [47].

A549 cells were seeded at a density of 200,000 cells/well in 6-well plates and left to attach overnight. After attachment, the cells were treated with 0 or 25 µM ribavirin for 72 hours. Following treatment, the cells were washed 3 times with ice-cold PBS, followed by lysis and harvesting with 400 µL radioimmunoprecipitation assay (RIPA) buffer (ThermoFisher Scientific, Australia) supplemented with protease inhibitor cocktail tablets (Roche Diagnostics, Switzerland). After lysis, the cells were centrifuged at 14,000 g for 15 minutes, at 3°C to separate insoluble cell membranes, and the cleared lysate was transferred into fresh tubes.

The protein concentration of each sample was determined *via* bicinchoninic A/acid (BCA) method (Pierce BCA kit, ThermoFisher Scientific, Australia), following the manufacturer's instructions.

The Proteome Profiler Human XL Protein Array Kit was used following the manufacturer's instructions, hybridizing 300 µg protein per sample in a final volume of 1.5 mL. The chemiluminescent signal was acquired using a ChemiDoc MP imaging system (Bio-Rad, USA), and the pixel density of each spot was quantified using the ImageJ software (version 1.53c, Bethesda, MD, USA).

2.8. Statistical Analysis

All data are shown as average ± SEM. Statistical analysis was performed using the PRISM v9.3 software (GraphPad, USA). Statistical comparisons were performed by either one-way ANOVA followed by Dunnet's test for pairwise comparisons, or by Student's t-test, as indicated in the figure legends. A P-value < 0.05 was considered statistically significant.

2.9. *In silico* studies

2.9.1. Gene Ontology & pathway enrichment analysis

Gene ontology (GO) mapping was performed to classify genes into a hierarchy of groups and to discover the gene regulatory network using biological functions and KEGG pathways. The DAVID computational biology tool (https://david.ncifcrf.gov/) was further utilized to evaluate gene ontology (GO) biological processes along with functional dominance. Also, the data set exhibited a p-value of 0.05 which was considered as a significant enrichment and ggplot2 was used to visualize the statistically most enriched GO terms [53].

2.9.2. Construction of PPI network

The protein-protein interaction (PPI) network is an intricate system in which proteins that participate in a biological event interact with one another. This network for the DEGs was identified using the GeneMANIA database and the PPI network was built with Cytoscape v3.7.1 which is a very effective tool for visualizing and analyzing PPI networks [54].

2.9.3. PPI network involving topological analysis

The topological qualities of the network as it has been formed are the first and main fundamental analysis as it aids in understanding the structure of a network, making it easier to comprehend the hidden mechanisms. The PPI network of genes' topological features are described by measurements of degree, centrality Betweenness (C_B), and BottleNeck (B_N). In this study, the topological properties were determined using Cytoscape plugins, Network Analyzer [55], and cytohubba [56] to understand topological changes that occur when the network is impacted. The following network properties were examined to investigate the network's essential behaviors.

a) Degree (***k***)***:*** The total number of linkages is established by a node in the network and indicated by the degree *k* during the network analysis process. This is also used to determine a node's local significance in the network regulation process. In the graph defined by *G = (N, E)*, *N* represents the nodes and E represents the edges. The degree of the i^{th} node (k_i) is represented as $k_i = \sum_{ij}^{N} A_{ij}$, where A_{ij} denotes the graph's adjacency matrix elements.

b) Betweenness centrality (C_B): The C_B, also known as betweenness centrality, is a node's share of all shortest-path traffic from all feasible routes through nodes i to j. As a result, it is the parameter of a node's ability to benefit from the flow of information throughout the network [57] and its capacity to regulate signal processing over other nodes in the network [58]. If $d_{ij}(v)$ indicates the number of geodesic lines from node i to node j that passing through node v, then $C_B(v)$ of node v can be calculated using equation 1.

$$C_b(v) = \sum_{i,j;i\neq j\neq k} \frac{d_{ij}(v)}{d_{ij}} \qquad \text{(Equation 1)}$$

The normalized betweenness centrality is summarized in the equation 2, in which M represents the number of node pairs, excluding v.

$$C_B(v) = \frac{1}{MC_b(v)} \qquad \text{(Equation 2)}$$

c) BottleNeck (B_N): The high betweenness nodes are the bottleneck, it can be estimated using central betweenness, which seems to be a measurement of the centrality of a node in a network, and equal to the number of shortest paths [56]. Let D n be the shortest node-rooted path tree, **(B_N)**

$$B_N(\mathbf{v}) = \sum \mathbf{x} \in \mathbf{VR_n(v)} \qquad \textbf{(4)}$$

where $R_n(v) = 1$ if more than $\frac{V(D_n)}{4}$ paths from node *n* to other nodes in D_n meet at the vertex v; otherwise $R_n(v) = 0$.

2.9.4. Driver gene identification

Centrality estimates can be utilized to identify essential driver genes by characterizing the most significant genes in a complex network, which are capable of quick information propagation, reception, and sensitivity to local and global alterations. To extract driver genes, the top ten genes with the highest degree, betweenness, and bottleneck centrality were used. To ensure their trustworthiness as regulatory network driver genes, the commons genes for the three topological qualities listed above were traced to the top 10 hub genes (genes with the highest degrees) [59-64].

2.9.5. Molecular docking

The Extra Precision (XP) tool in the Schrodinger suite's Glide programme was used for ligand docking. Both the produced protein and the ligand were obtained from Glide's Ligand Docking panel. We have downloaded the target protein pdb structures from RCSB PDB (https://www.rcsb.org/). The Ribavirin structure was downloaded from PubChem (https://pubchem.ncbi.nlm.nih.gov/), having CID: 37542. The protein's glide grid file and the suitably prepared ligand file were fed into the Ligand Docking panel, allowing for the exploration of protein-ligand interactions. Glide generated several stances automatically, subjecting them to multiple algorithmic screenings. The proteins and ligand were prepared by protein preparation vizard and Ligprep module of the GLIDE suite respectively. We have also used PDBSum server for identification of active site residues present in each crystal structures of proteins [65-67].

A grid minimization approach was used in the final screening stage to compute the OPLS-AA non-bonded ligand-protein interaction energy, identifying the poses with the lowest energy levels. These chosen poses with minimal energy were then displayed in the project table. A ligand interaction diagram was used to visualise the 2-D depiction of ligand-protein interactions, efficiently defining the interaction types with unique amino acids using a color-coded method. An overall study was performed to compare the observed binding affinity and interactions, with the goal of determining whether experimental molecule would serve as a superior ligand for Acetylcholinesterase [65]. The estimation of free energy for protein-ligand complexes utilising Prime's MM-GBSA panel required the use of prepared protein and ligand inputs. The programme generated output in the form of a maestro structure file, which included the MMGBSA_dG_Bind in Complex Energy values, allowing the free energy associated with the complexes to be assessed.

2.9.6. Molecular Dynamics (MD) simulation study

MD simulation stands as a prominently used computational method for modelling biological systems. In this study, we used GROMACS version 4.5.5 for conducting molecular dynamic simulations [68]. The Amber force field was used to build the protein's topology file, while the ACPYPE web service was used to generate topology files along with other essential parameter files for ligands [69]. All other processes and settings were consistent from earlier reports [70,

71]. In brief, our approach involved the solvation with spc water molecules to ensure electro-neutrality during the simulation and simultaneously Na/Cl counter ions were introduced.

Furthermore, the steepest descent approach, V-rescale temperature coupling, and Parrinello-Rahman pressure coupling were used to keep the system stable at 300 K and 1 bar. The Partial Mesh Ewald (PME) approach was used to estimate Van der Waals and electrostatic interactions. Also, the bond lengths were controlled using the LINCS technique and finally, both the complexes with apo-proteins were simulated for 100 ns.

We used the RMS (root mean square deviation), RMSF (root mean square fluctuation), and gyrate (radius of gyration) tools on the trajectory data to evaluate the behaviour of the backbone atoms throughout the simulations. The Graphing Advanced Computation and Exploration (GRACE) Programme was used to generate the plots.

3. Results

3.1 Antiproliferative activity of ribavirin on A549 cells and toxicity on BEAS-2B cells

To assess the antiproliferative activity of ribavirin on A549 human lung adenocarcinoma cells, and to determine its toxicity on non-cancerous BEAS-2B human bronchial epithelial cells, an MTT assay was performed after exposing both cell lines to concentrations of ribarivin ranging from 2.5 to 200 µM for 72 hours (**Figure 2**). On A549 cells, treatment with up to 10 µM ribavirin did not result in a significant reduction of cell proliferation (**Figure 2a**). Treatment with 25, 50, 75, 100, and 200 µM ribavirin resulted in a statistically significant, dose-dependent reduction of A549 cell proliferation of 12%, 26.9%, 33.3%, 43.5%, and 58.7%, respectively (**Figure 2a**). On BEAS-2B cells, treatment with up to 25 µM ribavirin did not significantly impact cell viability (**Figure 2b**). Treatment with 50, 75, 100, and 200 µM ribavirin resulted in a statistically significant, dose-dependent reduction of BEAS-2B cell viability of 30.3, 37.4, 44.7, and 53.6%, respectively (**Figure 2b**). Considering the absence of BEAS-2B cells toxicity

achieved by 25 µM ribavirin treatment, the subsequent experiments were performed treating A549 cells with 25 and µM ribavirin, or with 25 µM only in the case of the protein array.

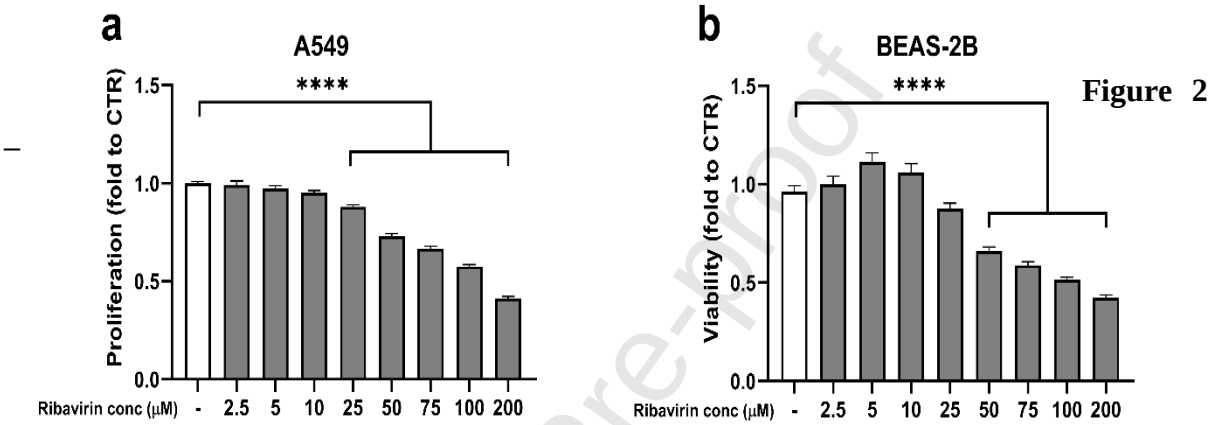

Figure 2

Assessment of the antiproliferative activity of ribavirin on A549 cells and its toxic effect on BEAS-2B cells. An MTT assay was performed to test the antiproliferative activity of ribavirin on A549 cells (**a**) and its toxic effect on BEAS-2B cells (**b**). 5,000 cells/well were seeded in a 96-well plate and treated for 72 hours with the indicated ribavirin concentrations. One-way ANOVA test, n=3, ****:$p<0.0001$.

3.2 Anti-migratory activity of ribavirin on A549 cells

To test the effect of ribavirin in inhibiting the migration of A549 cells, a wound healing assay was performed upon treating A549 cells with 25 µM ribavirin for up to 72 hours (**Figure 3**). At the 24-hour time point, the average wound closure of untreated cells was 42.3%, whereas the wound closure of cells treated with 25 µM ribavirin was 28.5% (**Figure 3a**). This corresponds to a statistically significant 32.6% reduction of the cells' migration achieved by 25 µM ribavirin (**Figure 3a**). At the 48-hour time point, the average wound closure of untreated cells was 55.6%, whereas the wound closure of cells treated with 25 µM ribavirin was 35.0% (**Figure 3b**). This corresponds to a statistically significant 37% reduction of the cells' migration achieved by 25 µM ribavirin (**Figure 3b**). At the 72-hour time point, the average wound closure

of untreated cells was 57.37%, whereas the wound closure of cells treated with 25 µM ribavirin was 36.6% (**Figure 3b**). This corresponds to a statistically significant 36.2% reduction of the cells' migration achieved by 25 µM ribavirin (**Figure 3c**). **Figure 3d** shows representative figures of the wound healing assay. Similarly, in our trans-well cell migration assay, we observed that 25 µM ribavirin treatment for 16 hours significantly inhibits the migration of A549 by 23.6% (p=0.0401 control vs 25 µM ribavirin) – **Figure 3e** and **Figure 3f**.

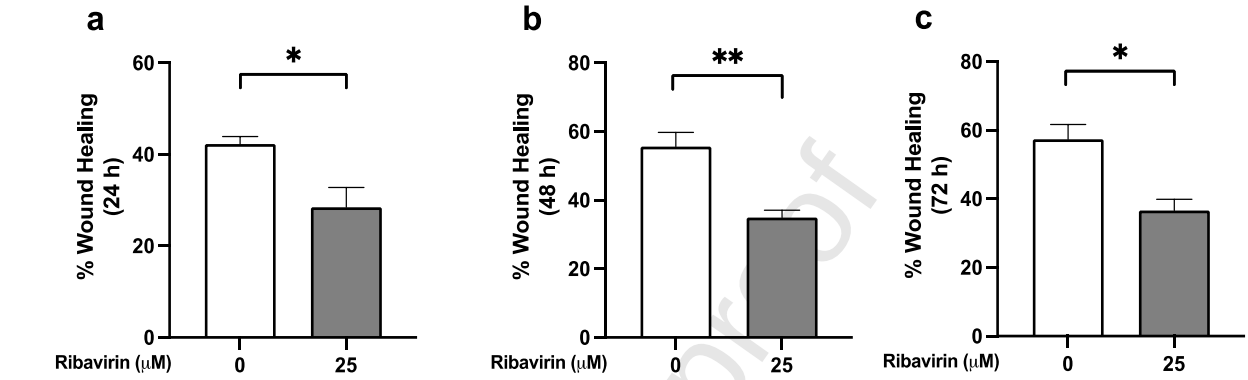

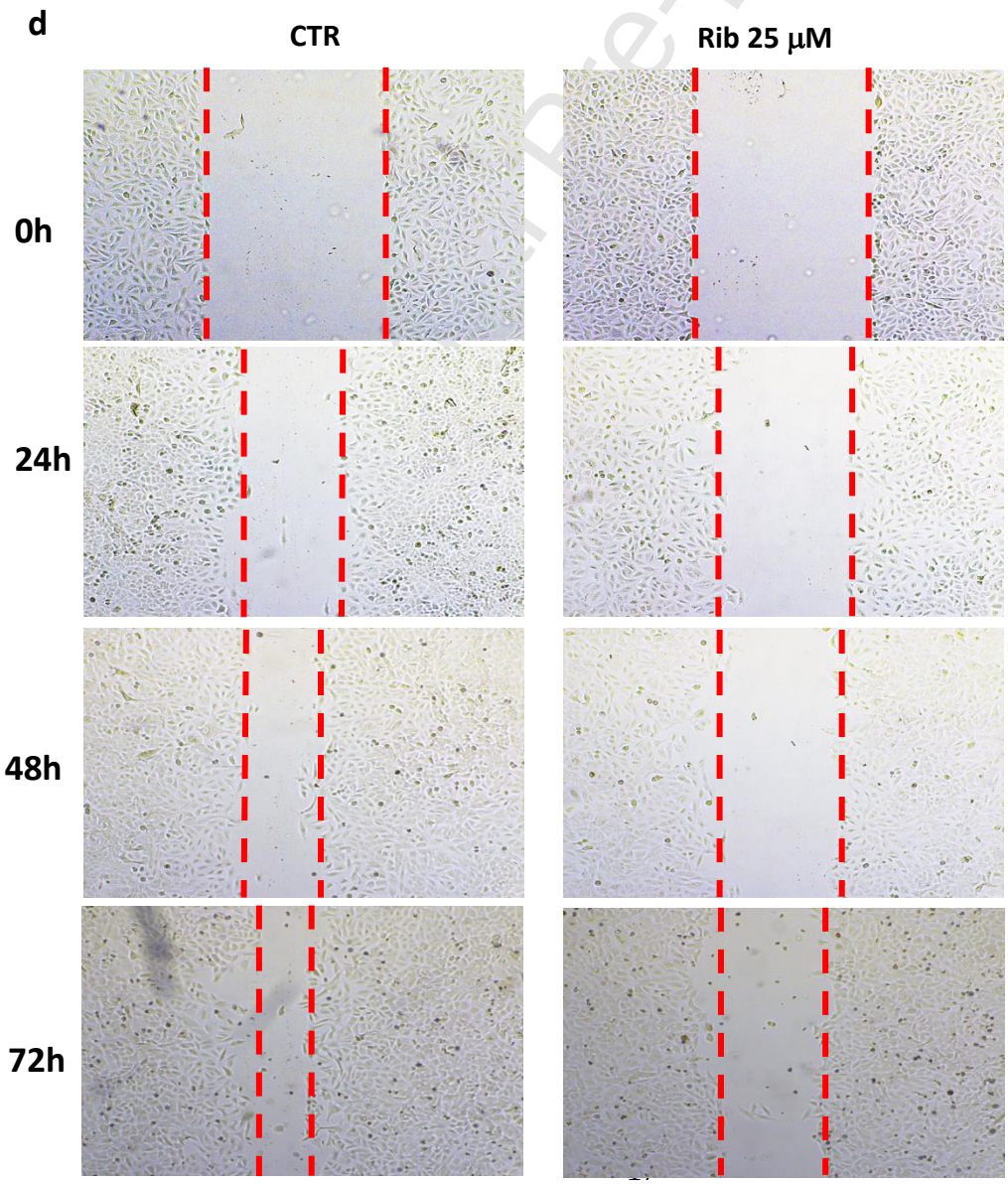

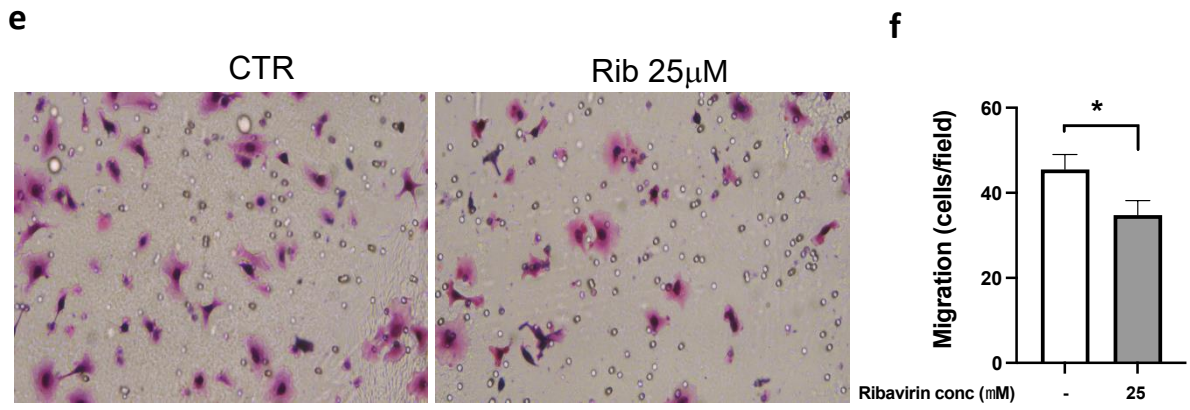

Figure 3 – Assessment of the anti-migratory activity of ribavirin on A549 cells – wound healing and transwell chamber migration assay

A wound healing assay was performed to test the anti-migratory activity of ribavirin on A549 cells upon 24 hours (**a**), 48 hours (**b**), and 72 hours (**c**) of treatment. Upon scratching a confluent monolayer of A549 cells in a 6-well plate, cells were treated with 25 µM ribavirin for up to 72 hours. **Figure 3d** shows representative pictures of the assay (**c**), scale bar = 300 µm. (**e**), Transwell cell migration assay on A549 cells treated with ribavirin and allowed for migration for 16 hours, followed by H/E staining, and microscopic images at 20X magnification (**f**) quantification of migrated cells per field. Statistical analysis was done with unpaired Student's t-test, n=3, *: $p<0.05$; **: $p<0.01$. CTR = control cells, Rib = Ribavirin (25 µM) treated cells

3.3 Anti-colony formation activity of ribavirin on A549 cells

To test the effect of ribavirin in inhibiting the formation of colonies in A549 cells, a colony formation assay followed by crystal violet staining was performed upon treating A549 cells, seeded at low density, with 25 µM ribavirin for 72 hours (**Figure 4**). After the period of treatment and colony development, the untreated cells developed an average of 88.3 colonies/well, whereas treatment with 25 µM ribavirin dose-dependently reduced the number of colonies developed to averages of 53.5 colonies/well (**Figure 4a**). This corresponds to a statistically significant 39.4% reduction of the colony formation capacity of A549 cells achieved by treatment with 25 µM ribavirin (**Figure 4a**). **Figure 4b** shows representative pictures of the colony formation assay.

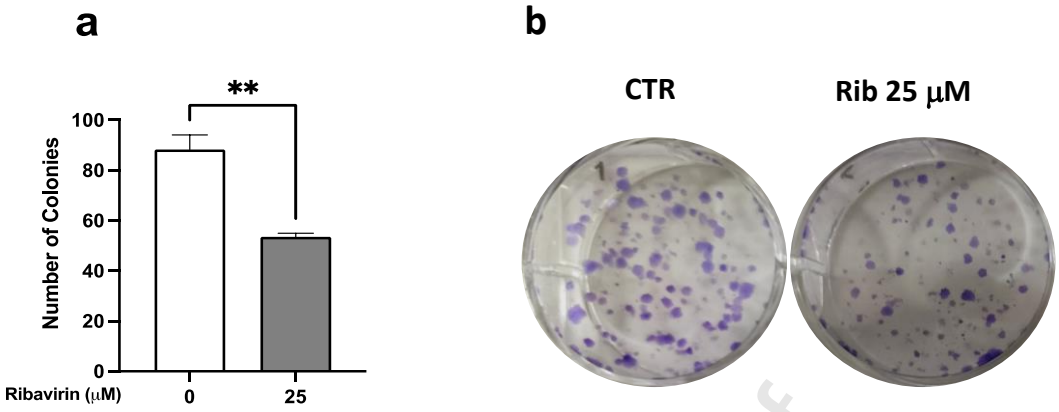

Figure 4 – Assessment of the anti-colony formation activity of ribavirin on A549 cells – colony formation assay

To assess the efficacy of ribavirin in inhibiting the capacity of A549 cells to form colonies when seeded at low density, A549 cells were seeded at a density of 500 cells/well in 6-well plates and treated with 25 μM ribavirin for 72 hours. After treatment, the cells were left to develop colonies for about two weeks and stained with crystal violet. (**a**) – Average number of colonies; (**b**) – representative pictures of the colony formation assay. Statistical analysis was done with unpaired Student's t-test, n=3, **: $p<0.01$. CTR = control cells, Rib = Ribavirin treated cells

3.4 Ribavirin treatment downregulates the mRNA expression of the oncogenes *KRAS* and *BRAF*

The effect of ribavirin on the expression of the oncogenes *KRAS* and *BRAF* was assessed by performing RT-qPCR after treating A549 cells with 25 μM ribavirin for 72 hours (**Figure 5**). Treatment with 25 μM ribavirin resulted in a statistically significant reduction of *KRAS* mRNA expression of 18.3% (**Figure 5a**). Treatment with 25 μM ribavirin resulted in a statistically significant reduction of *BRAF* mRNA expression of 32.1% (**Figure 5b**).

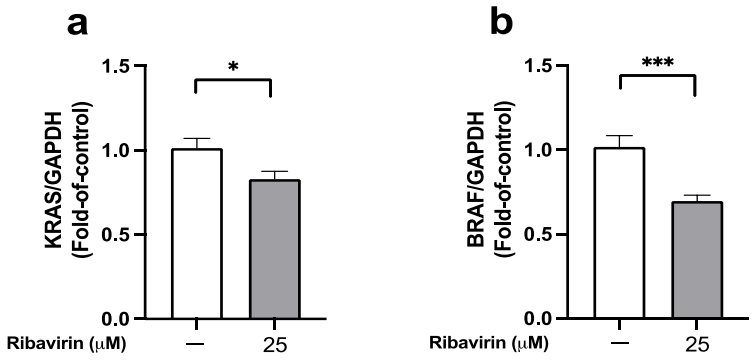

Figure 5 – Ribavirin downregulates the mRNA expression of the oncogenes *KRAS* and *BRAF* on A549 cells

To assess the effect of ribavirin on the expression of *KRAS* (**a**) and *BRAF* (**b**), an RT-qPCR was performed upon treating A549 cells with 25 µM ribavirin for 72 hours. Statistical analysis was done with unpaired Student's t-test, n=3; *: $p<0.05$; ***: $p<0.001$.

3.5 Ribavirin treatment downregulates the expression of proteins promoting cancer cell proliferation, migration/invasion/metastasis, and angiogenesis – oncology protein array analysis

To investigate the effect of ribarivin on the expression of proteins promoting cancer cell proliferation, migration, and angiogenesis, an oncology protein array evaluation was performed upon treating A549 cells with 25 µM ribavirin for 72 hours. The results are shown in **Figure 6** (proliferation), **Figure 7** (migration/invasion/metastasis), and **Figure 8** (angiogenesis).

3.5.1 Proteins promoting cell proliferation

Treatment with 25 µM ribavirin significantly reduced the expression of proteins promoting cell proliferation compared to the untreated control (**Figure 6**). In particular: the expression of ErbB4 was reduced by 85.8% (**Figure 6a**); the expression of enolase 3 was reduced by 14.4% (**Figure 6b**); the expression of CEACAM-5 was reduced by 84.8% (**Figure 6c**); the expression of ErbB3/HER3 was reduced by 49.1% (**Figure 6d**); the expression of SPARC was reduced by 46.7% (**Figure 6e**); and the expression of CA125/MUC16 was reduced by 82.1% (**Figure 6f**).

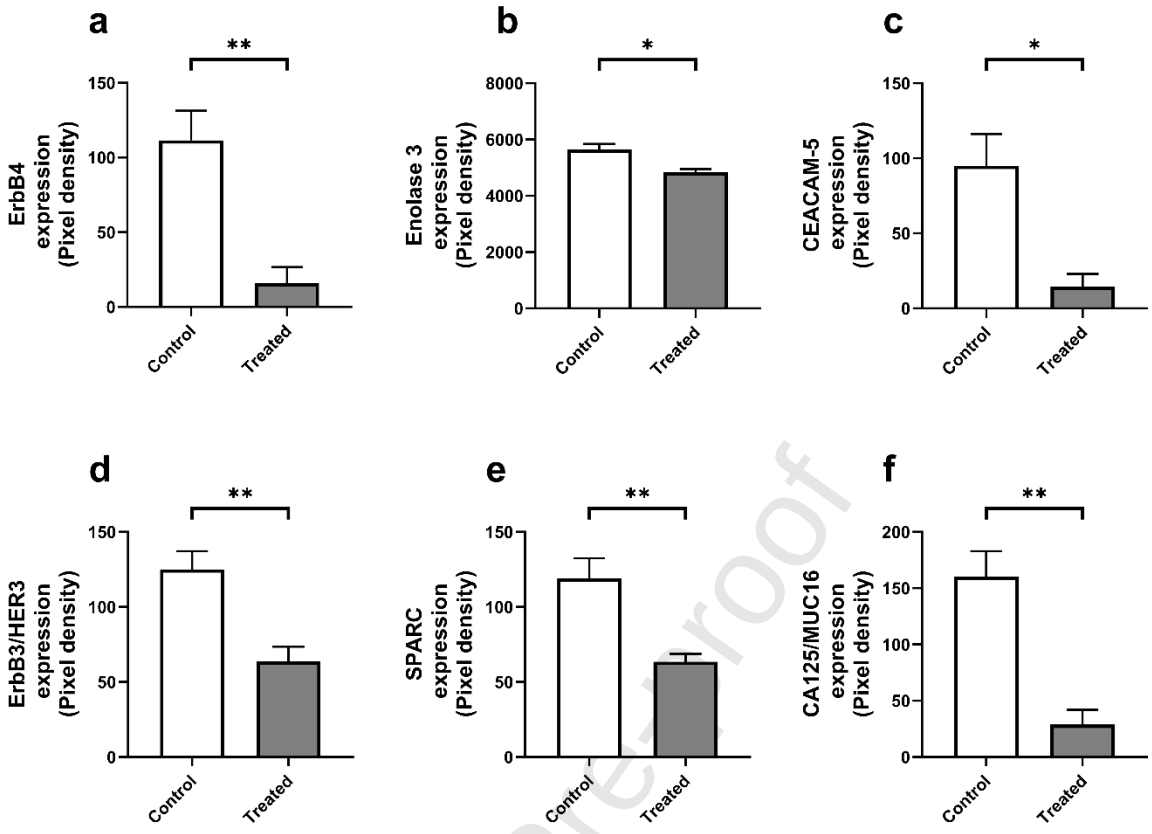

Figure 6 – Ribavirin downregulates the expression of proteins promoting A549 cells proliferation

To assess the effect of ribavirin on the expression of proteins promoting cancer cell proliferation, a protein array was performed on proteins extracted from A549 cells treated with 25 µM ribavirin for 72 hours. Ribavirin significantly reduced the expression of ErbB4 (**a**), enolase 3 (**b**), CEACAM-5 (**c**), ErbB3/HER3 (**d**), SPARC (**e**), and CA125/MUC16 (**f**). Unpaired Student's t-test, n=4, *: $p<0.05$; **: $p<0.01$.

3.5.2 Proteins promoting cell migration/invasion/metastasis

Treatment with 25 µM ribavirin significantly reduced the expression of proteins promoting cell migration, invasion, and metastasis compared to the untreated control (**Figure 7**). In particular: the expression of amphiregulin was reduced by 17.3% (**Figure 7a**); the expression of angiopoietin-like 4 was reduced by 96.3% (**Figure 7b**); the expression of CapG was reduced by 11.4% (**Figure 7c**); the expression of Thrombospondin-1 was reduced by 51.5% (**Figure 7d**); the expression of Tenascin C was reduced by 25.8% (**Figure 7e**); the expression of

mesothelin was reduced by 57.7% (**Figure 7f**); the expression of ENPP2-Autotaxin was reduced by 71.7% (**Figure 7g**); the expression of CCL7/MCP-3 was reduced by 64.3% (**Figure 7h**); the expression of carbonic anhydrase IX was reduced by 30.8% (**Figure 7i**); the expression of cathepsin B was reduced by 10.6% (**Figure 7j**); the expression of eNOS was reduced by 97.0% (**Figure 7k**); and the expression of ICAM-1/CD54 was reduced by 60.7% (**Figure 7l**).

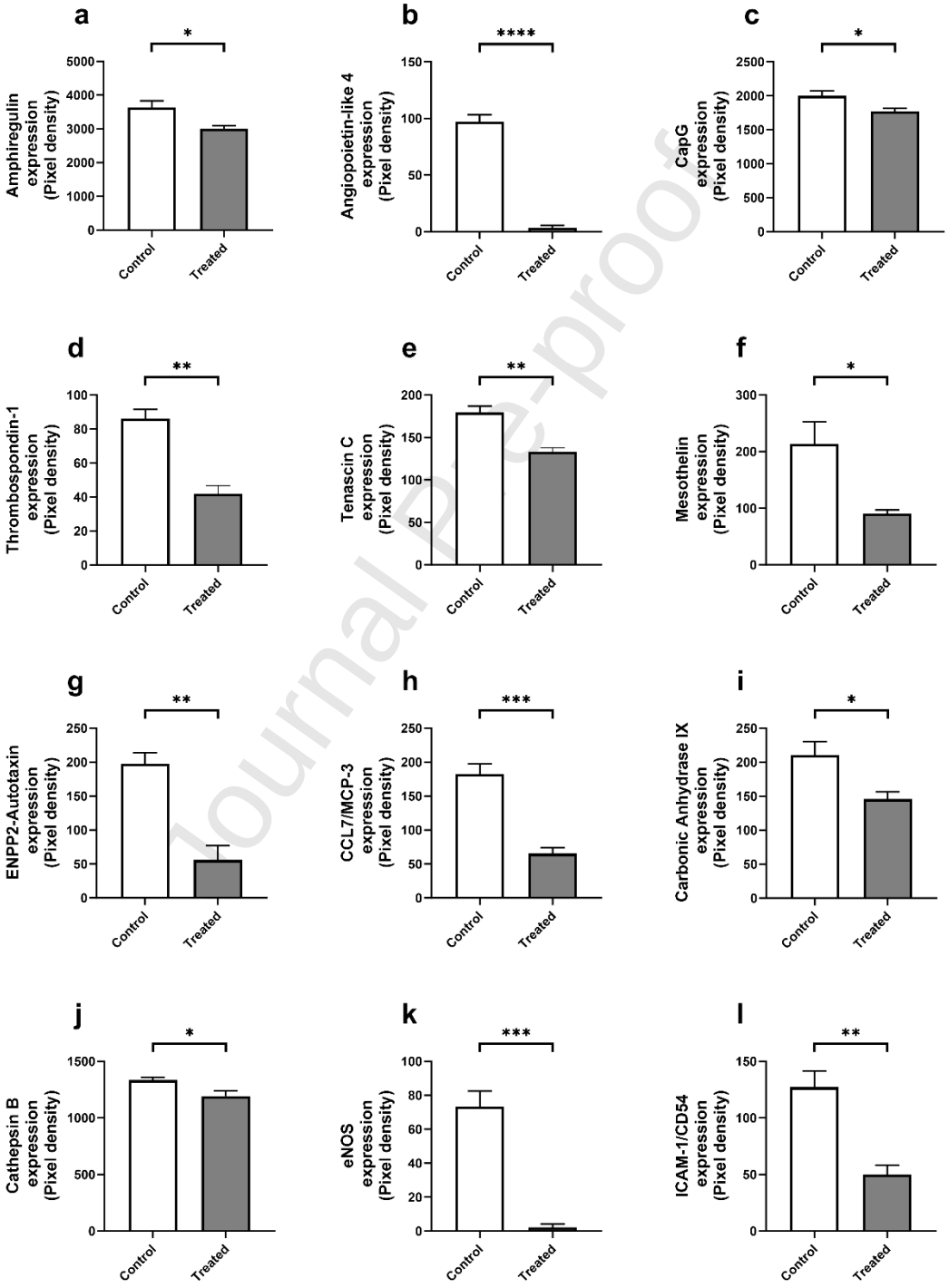

Figure 7 – Ribavirin downregulates the expression of proteins promoting A549 cells migration/invasion/metastasis

To assess the effect of ribavirin on the expression of proteins promoting cancer cell migration, invasion, and metastasis, a protein array was performed on proteins extracted from A549 cells treated with 25 µM ribavirin for 72 hours. Ribavirin significantly reduced the expression of amphiregulin (**a**), angiopoietin-like 4 (**b**), CapG (**c**), thrombospondin-1 (**d**), tenascin C (**e**), mesothelin (**f**), ENPP2-Autotaxin (**g**), CCL7/MCP-3 (**h**), carbonic anhydrase IX (**i**), cathepsin B (**j**), eNOS (**k**), and ICAM-1/CD54 (**l**). Unpaired Student's t-test, n=4, *: $p<0.05$; **: $p<0.01$; ***: $p<0.001$; ****: $p<0.0001$.

3.5.2 Proteins promoting angiogenesis

Finally, we investigated the effect of ribavirin on the expression of proteins regulating angiogenesis in cancer. Treatment with 25 µM ribavirin significantly reduced the expression of two of these proteins compared to the untreated control (**Figure 8**). In particular: the expression of VE-cadherin was reduced by 60.0% (**Figure 8a**); and the expression of HCG was reduced by 79.3% (**Figure 8b**).

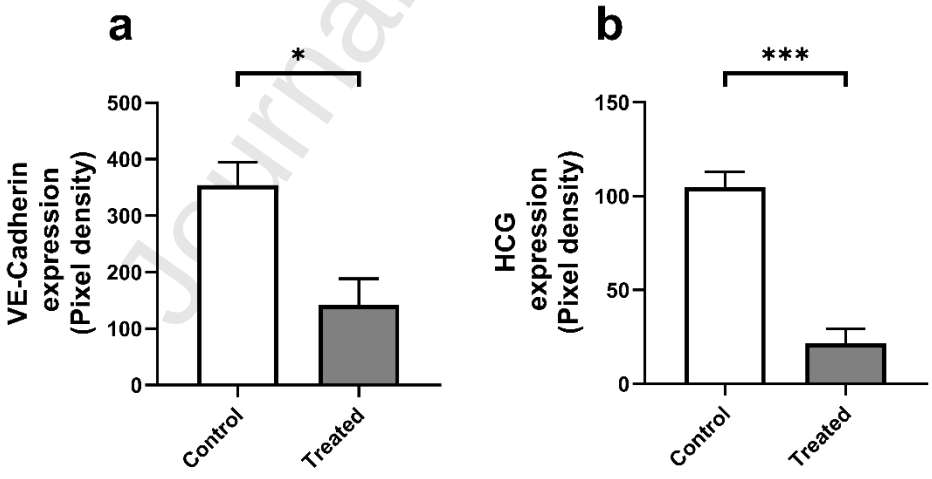

Figure 8 - Ribavirin downregulates the expression of proteins promoting angiogenesis in A549 cells

To assess the effect of ribavirin on the expression of proteins promoting angiogenesis, a protein array was performed on proteins extracted from A549 cells treated with 25 µM ribavirin for 72 hours. Ribavirin significantly reduced the expression of VE-cadherin (**a**) and HCG (**b**). Unpaired Student's t-test, n=4, *: $p<0.05$; ***: $p<0.001$.

3.6 In silico studies

3.6.1 Gene ontology and pathways of genes

Gene ontology enrichment analyses were performed to further explore the biological functions, cellular component, molecular function and KEGG pathways of genes. The biological process category of the GO analysis results showed that down-regulated genes were significantly enriched in immune response, cell proliferation, cell migration, apoptosis, angiogenesis, ERK1/K2 cascade, MAPK and Pi3K-Akt signaling pathways (**Figure 9**).

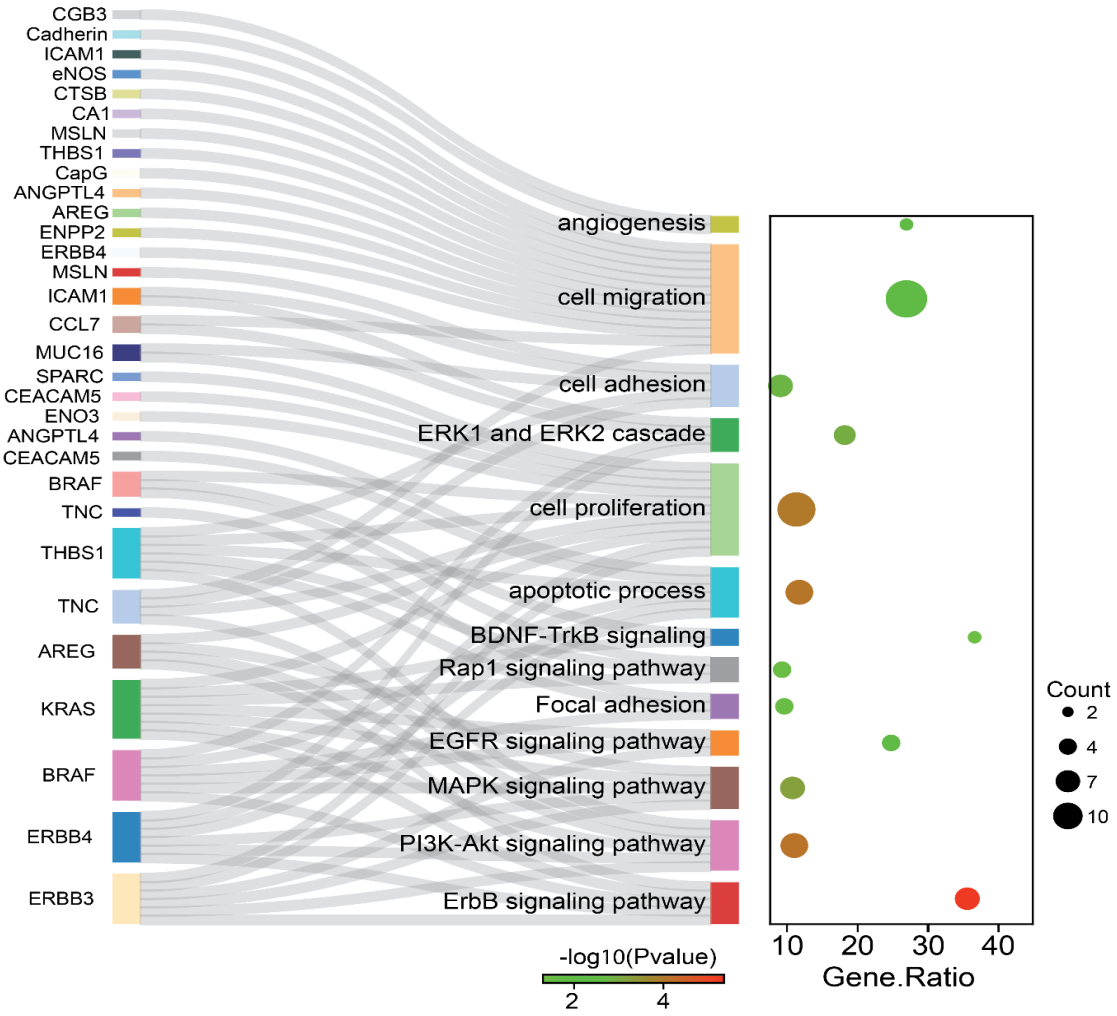

Figure 9 - Biological process and pathways of genes. The image illustrates the biological process and pathways of genes with Gene Ontology (GO) Enrichment Analysis of Down-regulated Genes.

Protein–Protein Interaction Network Construction and Downstream Analysis

In our analysis, a total of 24 genes involved in cell proliferation, cell migration, invasion, metastasis and angiogenesis were submitted to STRING for the construction and analysis of the network. The network analysis shows that the protein–protein interaction network has 45 interacting nodes and 140 edges (**Figure 10a**). Further analysis of this network was executed using Cytoscape. After performing the analysis, we found the top 10 hub genes (genes with highest degrees), KRAS, THBS1, ERBB4, ERBB3, AREG, CTSB, SPARC, NRG1, ICAM1 and BRAF as per the decreasing order of degree values. Furthermore, we identified the top 10 betweenness centrality genes NRG1, ICAM1, ERBB4, THBS1, KRAS, CTSB, CAPG, AREG, FSHB and CCR1 and the top 10 bottleneck genes NRG1, AREG, HER3, KRAS, eNOS, CCR1, ERBB4, ENO3, IGFBP5 and ICAM1, as per the decreasing order of highest betweenness centrality of score (**Figure 10b, 10c, and 10d**). The common genes for each pair are shown in Figure **10e**. Most of the hub genes in the network such as ERBB4, KRAS, AREG, NRG1, ICAM1, etc. are either associated with non-small cell lung cancer itself or other forms of cancers. We noted that cell proliferation, cell migration, invasion, metastasis and angiogenesis were some of the significant pathways for these key genes.

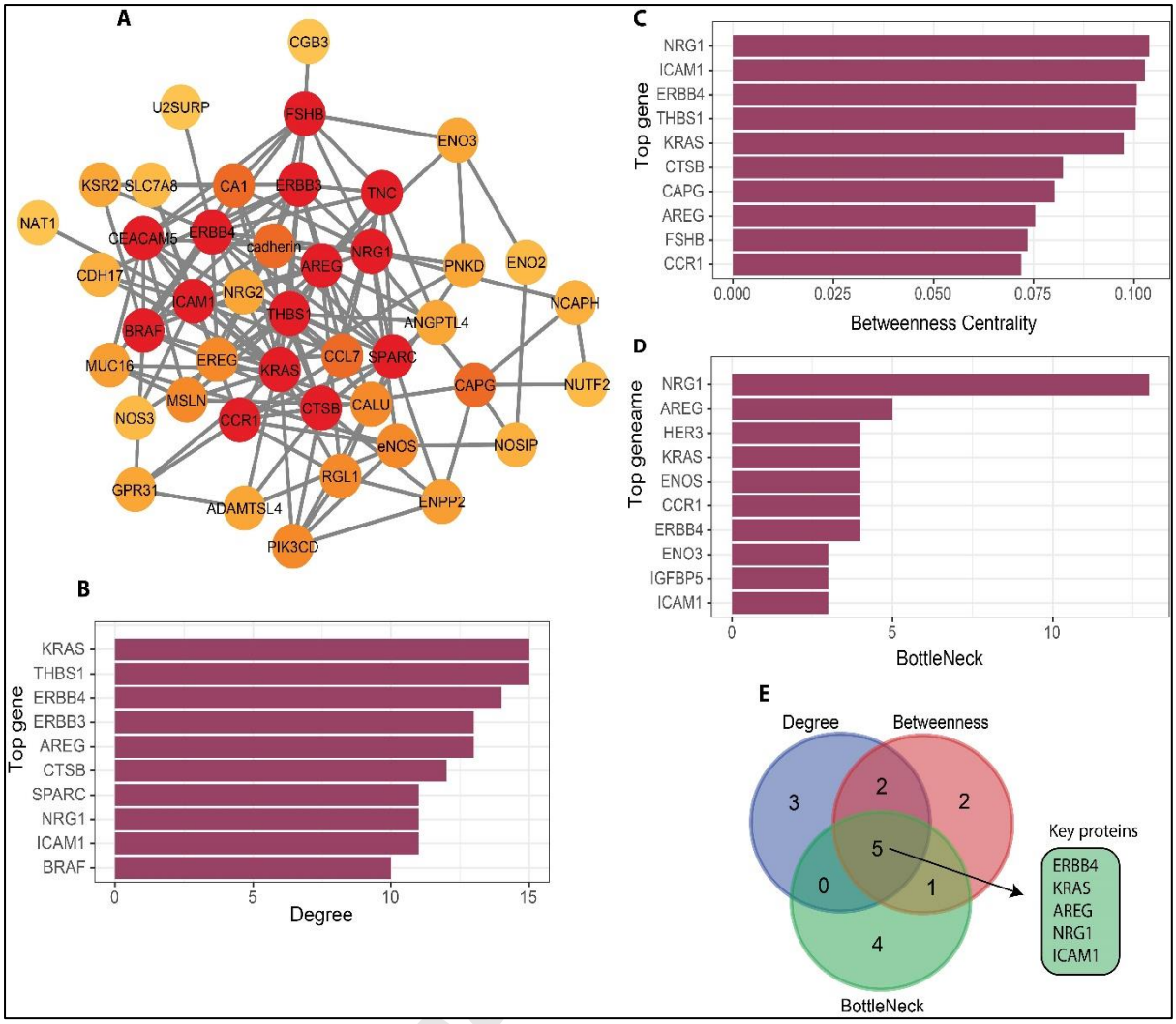

Figure 10: PPI regulatory network of genes: (**a**) Protein–protein network of genes. Color of nodes show the degree of notes, dark color showing higher value in analysis. (**b**) Bar graph of top 10 degree and (**c**) betweenness centrality (**d**) bottleneck genes of PPI network retrieved from significant modules (**e**) Venn diagram shows the number of common genes among various of top 10 genes topological parameters i.e., degree, betweenness centrality, and bottleneck. These common genes are considered as key genes.

3.6.2 Molecular Docking

Furthermore, we performed molecular docking study of key genes (i.e. ERBB4, KRAS,AREG, NRG1 and ICAM1) to Ribavirin. The binding energy of key genes with Ribavirin is given in **Table 1**. The molecular docking showed the highest binding energy of Ribavirin with the ERBB4 protein (**Table 1**). The binding energy was observed as -8.008 kcal/mol while the second ranked energy was -6.269 kcal/mol, made with KRAS interaction. The remaining

proteins, ICAM1, AREG, and NRG1 bound to ribavirin with an energy of -4.955 kcal/mol, -3.630 kcal/mol and -5.101 kcal/mol, respectively (**Table 1**). The docked complexes are shown in **Figure 11**.

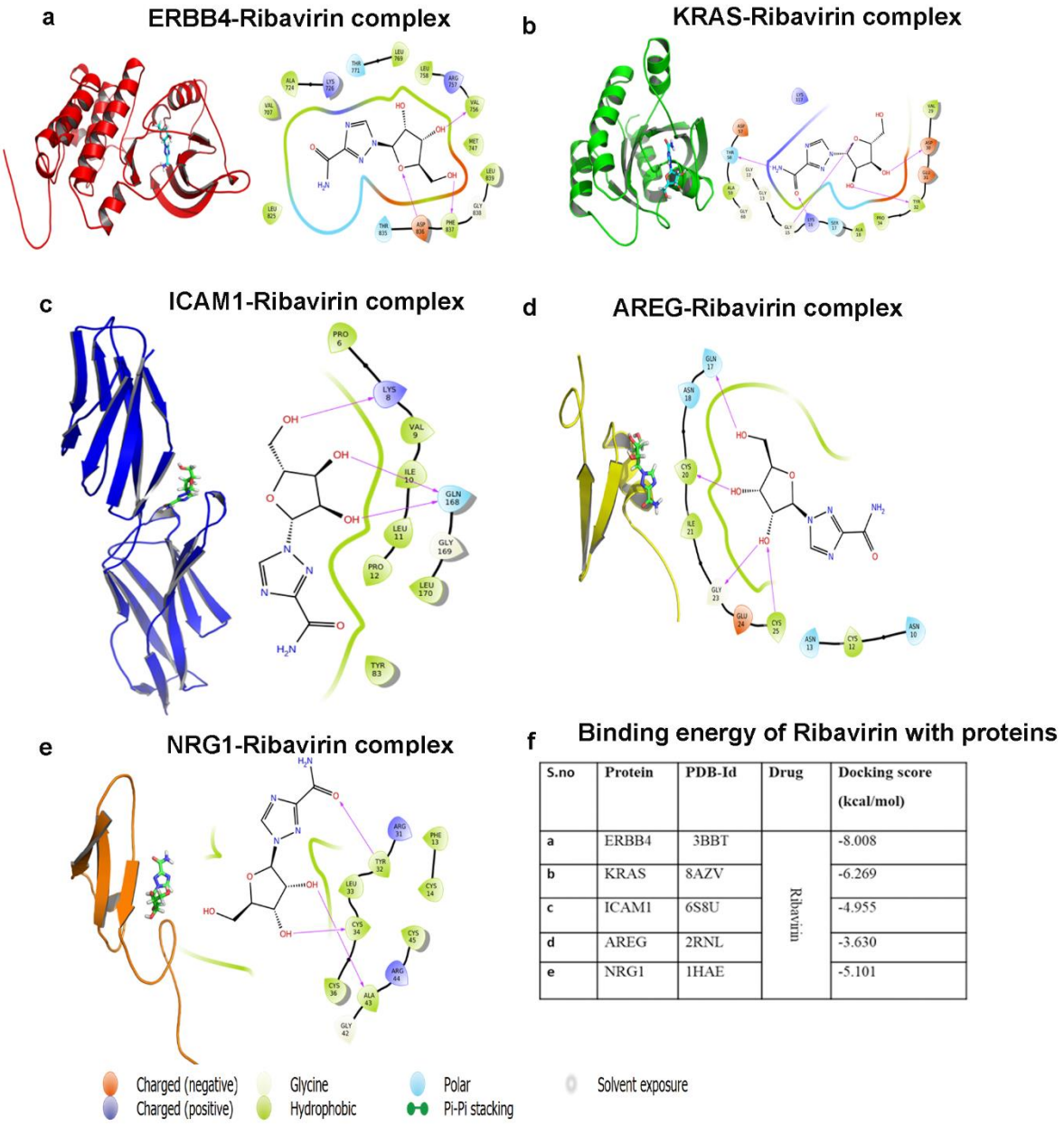

S.no	Protein	PDB-Id	Drug	Docking score (kcal/mol)
a	ERBB4	3BBT	Ribavirin	-8.008
b	KRAS	8AZV		-6.269
c	ICAM1	6S8U		-4.955
d	AREG	2RNL		-3.630
e	NRG1	1HAE		-5.101

Figure 11: Molecular docking analysis. Docking results of Ribavirin interaction with protein surface (**a**) ERBB4 (**b**) KRAS (**c**) ICAM1 (**d**) AREG (**e**) NRG1 (**f**) Binding energy of Ribavirin with proteins. Proteins are shown in cartoon and Ribavirin molecules are shown in stick model. Surrounding residues of ERBB4, KRAS, ICAM1, AREG and NRG1 proteins are shown.

3.6.3 MDS Results

The MD simulation analysis of ERBB4 & KRAS and their docked complexes (ERBB4-Ribavirin & KRAS-Ribavirin) are shown in **Figure 12** and **Figure 13** respectively. The backbone RMSD values of the entire systems rise throughout the earliest stages. Then ERBB4 apo-protein converged at 0.37 nm and its complex at 0.18 nm respectively during 100 ns (**Figure 12a**). Similarly, for KRAS apo-protein converged at 0.16 nm and its complex at 0.14 nm respectively during 100 ns (**Figure 13a**). The movement of each residue was disclosed by the RMSF value of the backbone residues in all the systems and were shown in **Figure 12b** and **Figure 13b,** respectively, whereas the volume of the tertiary structure and the compactness of the protein are explained by the Rg for all the systems, are represented in **Figure 12c** and **Figure 13c,** respectively.

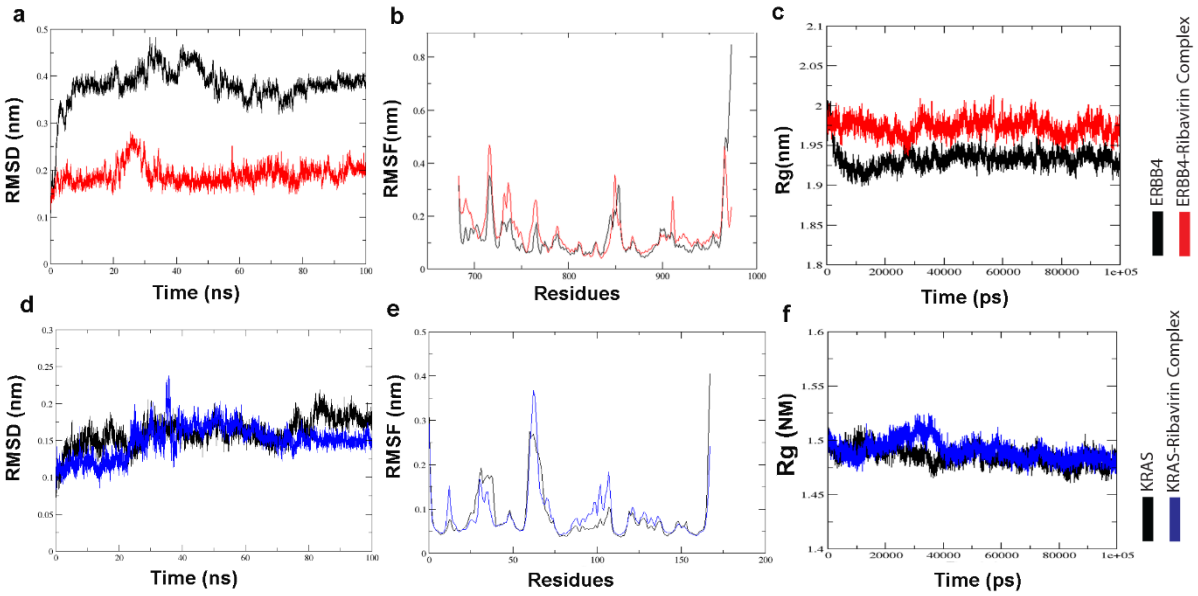

Figure 12: The results of molecular dynamics simulation. (**a**) The backbone RMSD of ERBB4 and complex of Ribavirin with protein ERBB4 for 100 ns MD simulation. (**b**) The backbone RMS fluctuation of ERBB4 and complex of Ribavirin with protein ERBB4, which clearly indicates four regions of ERBB4 fluctuate more. (**c**) Radius of gyration ERBB4 and complex of Ribavirin with protein ERBB4. (**d**) The backbone RMSD of KRAS and complex of Ribavirin with protein KRAS for 100 ns MD simulation. (**b**) The backbone RMS fluctuation of KRAS and complex of Ribavirin with protein KRAS, which clearly indicates four regions of KRAS fluctuate more. (**c**) Radius of gyration KRAS and complex of Ribavirin with protein KRAS.

4. Discussion

Drug repurposing is an exemplary approach for drug discovery [72]. In our study, we have re-purposed the anti-viral drug ribavirin for its anti-cancer potential in the human lung adenocarcinoma cell line A549. Through well-established and globally accepted *in vitro* techniques, we have demonstrated the anticancer activity of ribavirin through functional assays, mechanistic assays, and *in silico* studies.

Drug repurposing is associated with several advantages over discovering entirely novel compounds/drugs. This includes significantly reduced costs associated to research and development. Furthermore, the drug development timeframe is remarkably reduced because the Phase 1 clinical trials (safety) of existing, previously approved drugs is not required. Finally, some of these re-purposed drugs have potential for reuse despite evidence of adverse effects and failed efficacy in some indications [73]. In the present study, we chose an FDA-approved anti-viral drug, ribavirin, to investigate if it possesses anticancer activity against A549 cells. Recent literature has highlighted the anticancer therapeutic potential of ribavirin in different cancers, including acute myeloid leukemia, oropharyngeal squamous cell carcinoma, and metastatic breast cancer [36, 74, 75]. However, there is lack of literature claiming its anticancer activity against lung cancer. Therefore, we aimed at exploring the anti-lung cancer activity of ribavirin.

In our study, we observed potent anti-proliferative and anti-migratory activity of ribavirin *in vitro*. Through functional assays such as the MTT cell proliferation assay (**Figure 2**), the wound healing assay (**Figure 3a-d**), transwell cell migration assay (**Figure 3e, 3f**) and the colony formation assay (**Figure 4**), we showed that ribavirin at a dose of 25 μM exert remarkable anti-proliferative, anti-migration, and anti-colony formation activity. It is well known that anti-cancer agents also kill normal/healthy cells. For this reason, it is important to optimize the concentration of these anti-cancer drugs in order to identify a certain concentration which maximizes inhibition of cancer cell proliferation while being relatively safe for healthy cells to avoid or minimize the incidence of any potential side effects. It is clear from figure 2 that a concentration of 25 μM Ribavirin is toxic to A549 cells (****$p<0.0001$ compared to control), while the same concentration is safe in BEAS-2B cells (control versus 25 μM Ribavirin is non-significant). Therefore, we can assume that up to 25 μM Ribavirin do not possess significant side effects to the healthy cells but greater than 25 μM Ribavirin is toxic and it will have side effect to normal cells. From this we can clearly understand that the

optimum concentration we can use Ribavirin to assess its anti-cancer activity without causing side effect to healthy cells is 25 μM. To validate if the anti-cancer activity of 25 μM Ribavirin on A549 lung cancer cell is reproducible in another lung cancer cell line, we performed the proliferation (MTT assay) and migration (wound healing) assays on larger cell lung cancer cell line H460. In line with our findings with A549, Ribavirin at a concentration of 25 μM significantly inhibited the proliferation (**supplementary figure S1**) and migration (**supplementary figure S2a, S2b, and S2c**). Our functional assay was supported by mechanistic assays aimed at exploring the protein and gene expression. With regards to gene expression, we observed that ribavirin at a dose of 25 μM significantly decreased the mRNA expression of *KRAS* (**Figure 5a**) and *BRAF* (**Figure 5b**). Inhibition of KRAS-dependent lung cancer cell proliferation and blockage of autophagy to increases cytotoxicity represents potential approach to control lung cancer progression [76]. Similarly, BRAF inhibitors are promising drug candidates in the management of lung cancer [77]. This clearly suggests that ribavirin is a potent anti-cancer agent to control proliferation of lung cancer. Similarly, in terms of protein expression, we have observed that ribavirin notably inhibits the key protein such as ErbB4, ErbB3/HER3, Enolase 3, CECAM-5, SPARC, CA125/MUC16, involved in cancer cell proliferation (**Figure 7**). Likewise, ribavirin also inhibited the expression of key protein involved in cancer cell migration/invasion/metastasis, including Amphiregulin, Angiopoietin-like 4, CapG, Thrombospondin-1, Tenascin C, Mesothelin, ENPP2-Autotaxin, CCL7/MCP-3, Carbonic anhydrase IX, Cathepsin B, eNOS, ICAM-1/CD54 (**Figure 8**). On top of that, ribavirin also inhibited the protein expression of two key protein involved in angiogenesis: VE-cadherin and HCD (**Figure 9**). The findings reported in the present manuscript are in agreement with a recent study from our team, whereby we demonstrated that ribavirin reduces the production of IL-6 and IL-8 in A549 cells, two cytokines implicated in the promotion of various stages of cancer progression [37].

To further validate our *in vitro* findings, we performed *in silico* analysis using integrative network analysis, molecular docking and molecular dynamic simulation. We performed gene ontology and downstream analysis of genes and observed that ERBB4, KRAS, ICAM1, AREG and NRG1 were the key proteins identified. Amongst them, ERBB4 receptors showed the highest binding conformity with the target. These are the same proteins identified that support the anti-proliferative activity of ribavirin in our protein array data. Furthermore, various research studies have recognised ERBB4 for serving significant functions in a variety of cellular events, including proliferation, differentiation, angiogenesis, and apoptosis. A

functional assessment of its nine variants has revealed that there are four types of activating mutations (K935I, D931Y, Y285C, and D595V) causing increased basal and ligand-induced ERBB4 phosphorylation [78]

Also, ERBB4 and NRG1 polymorphisms have been substantially linked to an elevated probability of developing lung cancer, implying a possible susceptibility to lung cancer formation due to ERBB4 mutation [79]. The current study's findings provide further evidence supporting ERBB4's major role in human lung cancer and propose it as a viable molecular target for anticancer therapy.

In spite of the fact that docking studies have been effectively utilized in computing the limiting postures of ligands for some proteins, they refrained in evaluating ligand potential to binding. The protein rigidity in consideration overlooks the conformational modification in the course of docking of certain ligands [80]. The modifications in conformation during protein–ligand interactions could be contemplated through MD trajectory reproductions. The conformity changes in interaction of protein–ligand have been comprehensively examined through MD simulation strategies. With the substantial proliferation of computational biology, utilizing bioinformatics tools has forced stringent compliance in drug designing, thus helping to reduce the expenses and turn over time needed for *in vivo* screening and experimentations prerequisite for successful drug development [81]. These approaches have culminated in real-life outcomes including drug candidates recognition, structure-based designing and screening of the drug molecule, and genome-based investigation to locate host-specific targets [82].

Recently, computational skills determined the probability of linking various molecules before their development and estimation in experimental setup. Thus, the top-ranked compounds further chosen for MD simulation which demonstrated outcomes within the acceptable range of parameters proposes the interaction results are reliable in conformation. Nonetheless, investigative efforts on drug-gene interactions in our work, potentially inspire the research activities to identify therapeutic drug candidates for lung cancer.

The results of the present study are summarized in **Figure 13**, which also serves as a graphical abstract of the study.

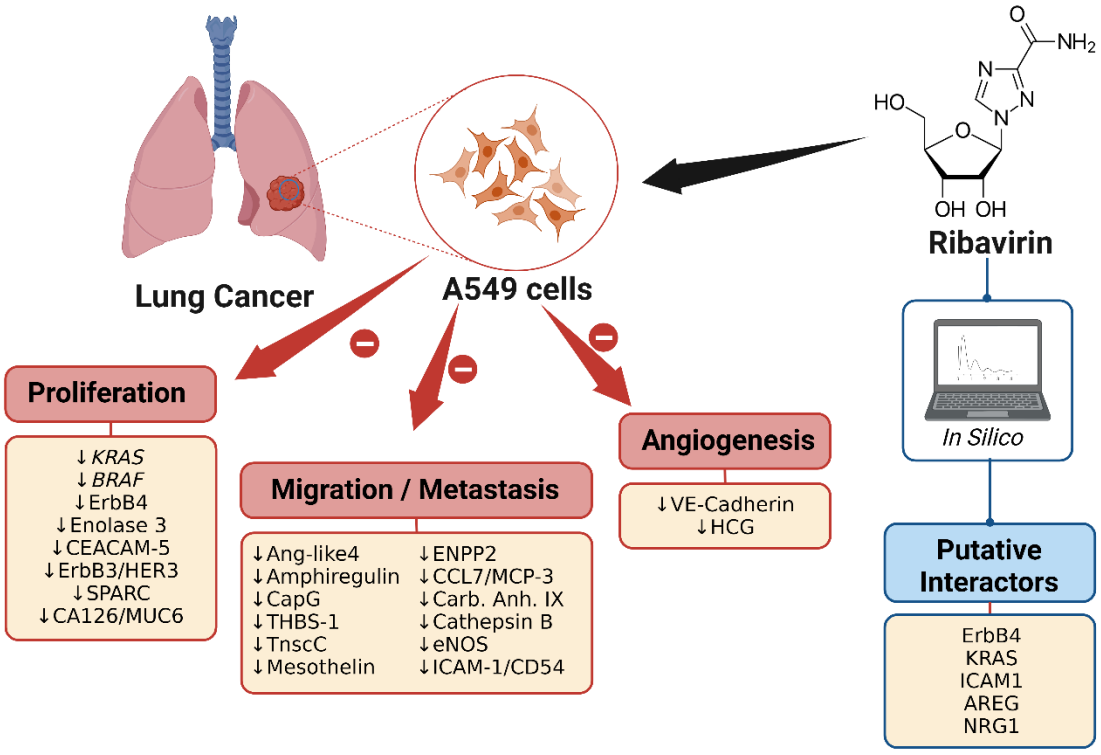

Figure 13 – Summary of the findings of the study highlighting the molecular pathways impacted by ribavirin as part of its *in vitro* anticancer activity on A549 cells

Although we showed very promising biological activity of ribavirin against A549 lung cancer cells *in vitro* and *in silico*, there are certain limitations in our study that would serve as a research platform to expand our hypothesis. Our study lacks the inclusion of *in vivo* animal models of lung cancer to correlate the *in vitro* and *in silico* data. Similarly, it would be interesting to expand our study using 3D culture system such as lung-on-a-chip or microfluidics systems, that allows growing multiple cell types such as macrophage and fibroblasts, creating a tumour microenvironment that could mimic more realistically the physiological condition. Another potentially interesting study would involve assessing the potential of ribavirin on three-dimensional spheroid cancer models. Nevertheless, our study suggests that with further strengthening of research with ribavirin, it can be re-purposed as a valid therapeutic option for lung cancer.

5. Conclusions

In conclusion, the results of the present study highlight the promising activity of ribavirin, an antiviral molecule, for the treatment of lung cancer. The findings showcased in this study, if confirmed by further *in vitro, in vivo,* and clinical investigations, will provide a platform for the repurposing of ribavirin as a monotherapy or as an adjuvant therapy for the treatment of lung cancer.

6. Declarations

Availability of data and material

Inquiries can be directed to the corresponding author.

6.1. Funding

KD is supported by a project grant from the Rebecca L Cooper Medical Research Foundation and the Maridulu Budyari Gumal Sydney Partnership for Health, Education, Research and Enterprise (SPHERE) RSEOH CAG Seed grant, fellowship and extension grant and the UTS Faculty of Health MCR/ECR Mentorship Support Grant. KRPs is supported by a joint fellowship from Prevent Cancer Foundation and International Association for the Study of Lung Cancer (IASLC) USA. KD, GDR, and KRP are supported by the Maridulu Budyari Gumal Sydney Partnership for Health, Education, Research and Enterprise (SPHERE) RSEOH CAG and Triple I Seed and extension grants, Triple I Skills Advancement Grants 2023 and the UTS Faculty of Health Industry Partnership Grant. GDR and KD are also supported by the UTS 2023 Key Technology Partner (KTP) grants.

6.2. Conflicts of Interest

The authors declare that the research was conducted without any financial or commercial relationships that could be interpreted as a potential conflict of interest.

6.3. Ethics approval and informed consent

Not applicable

References

1. Herbst RS, Heymach JV, Lippman SM. Lung cancer. N Engl J Med. 2008;359(13):1367-80; doi: 10.1056/NEJMra0802714.
2. Mehta M, Dhanjal DS, Paudel KR, Singh B, Gupta G, Rajeshkumar S, et al. Cellular signalling pathways mediating the pathogenesis of chronic inflammatory respiratory diseases: an update. Inflammopharmacology. 2020;28(4):795-817; doi: 10.1007/s10787-020-00698-3.
3. Sung H, Ferlay J, Siegel RL, Laversanne M, Soerjomataram I, Jemal A, et al. Global Cancer Statistics 2020: GLOBOCAN Estimates of Incidence and Mortality Worldwide for 36 Cancers in 185 Countries. CA Cancer J Clin. 2021;71(3):209-49; doi: 10.3322/caac.21660.
4. Wong MCS, Lao XQ, Ho KF, Goggins WB, Tse SLA. Incidence and mortality of lung cancer: global trends and association with socioeconomic status. Sci Rep. 2017;7(1):14300; doi: 10.1038/s41598-017-14513-7.
5. Malyla V, Paudel KR, Shukla SD, Donovan C, Wadhwa R, Pickles S, et al. Recent advances in experimental animal models of lung cancer. Future Med Chem. 2020;12(7):567-70; doi: 10.4155/fmc-2019-0338.
6. Paudel KR, Panth N, Pangeni R, Awasthi R, Chawla V, Mehta M, et al. Targeting lung cancer using advanced drug delivery systems. In: Targeting chronic inflammatory lung diseases using advanced drug delivery systems. Elsevier; 2020. p. 493-516.
7. Hardwick J, Taylor J, Mehta M, Satija S, Paudel KR, Hansbro PM, et al. Targeting Cancer using Curcumin Encapsulated Vesicular Drug Delivery Systems. Curr Pharm Des. 2021;27(1):2-14; doi: 10.2174/1381612826666200728151610.
8. Mehta M, Malyla V, Paudel KR, Chellappan DK, Hansbro PM, Oliver BG, et al. Berberine loaded liquid crystalline nanostructure inhibits cancer progression in adenocarcinomic human alveolar basal epithelial cells in vitro. J Food Biochem. 2021;45(11):e13954; doi: 10.1111/jfbc.13954.
9. Paudel KR, Jha SK, Allam V, Prasher P, Gupta PK, Bhattacharjee R, et al. Recent Advances in Chronotherapy Targeting Respiratory Diseases. Pharmaceutics. 2021;13(12); doi: 10.3390/pharmaceutics13122008.
10. Wadhwa R, Paudel KR, Chin LH, Hon CM, Madheswaran T, Gupta G, et al. Anti-inflammatory and anticancer activities of Naringenin-loaded liquid crystalline nanoparticles in vitro. J Food Biochem. 2021;45(1):e13572; doi: 10.1111/jfbc.13572.
11. Alnuqaydan AM, Almutary AG, Azam M, Manandhar B, De Rubis G, Madheswaran T, et al. Phytantriol-Based Berberine-Loaded Liquid Crystalline Nanoparticles Attenuate Inflammation and Oxidative Stress in Lipopolysaccharide-Induced RAW264.7 Macrophages. Nanomaterials (Basel). 2022;12(23); doi: 10.3390/nano12234312.
12. Khursheed R, Dua K, Vishwas S, Gulati M, Jha NK, Aldhafeeri GM, et al. Biomedical applications of metallic nanoparticles in cancer: Current status and future perspectives. Biomed Pharmacother. 2022;150:112951; doi: 10.1016/j.biopha.2022.112951.
13. Mehta M, Satija S, Paudel KR, Malyla V, Kannaujiya VK, Chellappan DK, et al. Targeting respiratory diseases using miRNA inhibitor based nanotherapeutics: Current status and future perspectives. Nanomedicine: Nanotechnology, Biology and Medicine. 2021;31:102303.
14. Hanahan D, Weinberg RA. Hallmarks of cancer: the next generation. Cell. 2011;144(5):646-74; doi: 10.1016/j.cell.2011.02.013.
15. Solanki N, Mehta M, Chellappan DK, Gupta G, Hansbro NG, Tambuwala MM, et al. Antiproliferative effects of boswellic acid-loaded chitosan nanoparticles on human lung

cancer cell line A549. Future Med Chem. 2020;12(22):2019-34; doi: 10.4155/fmc-2020-0083.
16. Wadhwa R, Paudel KR, Shukla S, Shastri M, Gupta G, Devkota HP, et al. Epigenetic therapy as a potential approach for targeting oxidative stress–induced non-small-cell lung cancer. Handbook of oxidative stress in cancer: Mechanistic aspects. 2020:1-16.
17. Kim E, Kim YJ, Ji Z, Kang JM, Wirianto M, Paudel KR, et al. ROR activation by Nobiletin enhances antitumor efficacy via suppression of IkappaB/NF-kappaB signaling in triple-negative breast cancer. Cell Death Dis. 2022;13(4):374; doi: 10.1038/s41419-022-04826-5.
18. Devkota HP, Adhikari-Devkota A, Paudel KR, Panth N, Chellappan DK, Hansbro PM, et al. Tea (Catechins Including (−)-Epigallocatechin-3-Gallate) and Cancer. Nutraceuticals and Cancer Signaling: Clinical Aspects and Mode of Action. 2021:451-66.
19. Siddiqui S, Deshmukh AJ, Mudaliar P, Nalawade AJ, Iyer D, Aich J. Drug repurposing: re-inventing therapies for cancer without re-entering the development pipeline—a review. Journal of the Egyptian National Cancer Institute. 2022;34(1):33; doi: 10.1186/s43046-022-00137-0.
20. De Rubis G, Bebawy M. Extracellular Vesicles in Chemoresistance. Subcell Biochem. 2021;97:211-45; doi: 10.1007/978-3-030-67171-6_9.
21. Al-Dimassi S, Abou-Antoun T, El-Sibai M. Cancer cell resistance mechanisms: a mini review. Clinical and Translational Oncology. 2014;16(6):511-6; doi: 10.1007/s12094-014-1162-1.
22. Doan TL, Pollastri M, Walters MA, Georg GI. Chapter 23 - The Future of Drug Repositioning: Old Drugs, New Opportunities. In: Macor JE, editor. Annual Reports in Medicinal Chemistry. Academic Press; 2011. p. 385-401.
23. Mercorelli B, Palù G, Loregian A. Drug Repurposing for Viral Infectious Diseases: How Far Are We? Trends Microbiol. 2018;26(10):865-76; doi: 10.1016/j.tim.2018.04.004.
24. Krishnamurthy N, Grimshaw AA, Axson SA, Choe SH, Miller JE. Drug repurposing: a systematic review on root causes, barriers and facilitators. BMC Health Services Research. 2022;22(1):970; doi: 10.1186/s12913-022-08272-z.
25. Pillaiyar T, Meenakshisundaram S, Manickam M, Sankaranarayanan M. A medicinal chemistry perspective of drug repositioning: Recent advances and challenges in drug discovery. European Journal of Medicinal Chemistry. 2020;195:112275; doi: https://doi.org/10.1016/j.ejmech.2020.112275.
26. Mehndiratta S, Qian B, Chuang JY, Liou JP, Shih JC. N-Methylpropargylamine-Conjugated Hydroxamic Acids as Dual Inhibitors of Monoamine Oxidase A and Histone Deacetylase for Glioma Treatment. J Med Chem. 2022;65(3):2208-24; doi: 10.1021/acs.jmedchem.1c01726.
27. Shaimerdenova M, Karapina O, Mektepbayeva D, Alibek K, Akilbekova D. The effects of antiviral treatment on breast cancer cell line. Infectious Agents and Cancer. 2017;12(1):18; doi: 10.1186/s13027-017-0128-7.
28. Chow WA, Jiang C, Guan M. Anti-HIV drugs for cancer therapeutics: back to the future? Lancet Oncol. 2009;10(1):61-71; doi: 10.1016/s1470-2045(08)70334-6.
29. Chen X, Wang C, Guan S, Liu Y, Han L, Cheng Y. Zidovudine, abacavir and lamivudine increase the radiosensitivity of human esophageal squamous cancer cell lines. Oncol Rep. 2016;36(1):239-46; doi: 10.3892/or.2016.4819.
30. Subeha MR, Telleria CM. The Anti-Cancer Properties of the HIV Protease Inhibitor Nelfinavir. Cancers (Basel). 2020;12(11); doi: 10.3390/cancers12113437.

31. Tong S, Su Y, Yu Y, Wu C, Chen J, Wang S, et al. Ribavirin therapy for severe COVID-19: a retrospective cohort study. International Journal of Antimicrobial Agents. 2020;56(3):106114; doi: https://doi.org/10.1016/j.ijantimicag.2020.106114.
32. Pfab C, Schnobrich L, Eldnasoury S, Gessner A, El-Najjar N. Repurposing of Antimicrobial Agents for Cancer Therapy: What Do We Know? Cancers (Basel). 2021;13(13); doi: 10.3390/cancers13133193.
33. Huq S, Casaos J, Serra R, Peters M, Xia Y, Ding AS, et al. Repurposing the FDA-Approved Antiviral Drug Ribavirin as Targeted Therapy for Nasopharyngeal Carcinoma. Molecular Cancer Therapeutics. 2020;19(9):1797-808; doi: 10.1158/1535-7163.Mct-19-0572.
34. De la Cruz-Hernandez E, Medina-Franco JL, Trujillo J, Chavez-Blanco A, Dominguez-Gomez G, Perez-Cardenas E, et al. Ribavirin as a tri-targeted antitumor repositioned drug. Oncol Rep. 2015;33(5):2384-92; doi: 10.3892/or.2015.3816.
35. Shen X, Zhu Y, Xiao Z, Dai X, Liu D, Li L, et al. Antiviral Drug Ribavirin Targets Thyroid Cancer Cells by Inhibiting the eIF4E-β-Catenin Axis. Am J Med Sci. 2017;354(2):182-9; doi: 10.1016/j.amjms.2017.03.025.
36. Casaos J, Gorelick NL, Huq S, Choi J, Xia Y, Serra R, et al. The Use of Ribavirin as an Anticancer Therapeutic: Will It Go Viral? Mol Cancer Ther. 2019;18(7):1185-94; doi: 10.1158/1535-7163.MCT-18-0666.
37. De Rubis G, Paudel KR, Yeung S, Agarwal V, Hansbro PM, Oliver BGG, et al. Ribavirin attenuates carcinogenesis by downregulating IL-6 and IL-8 in vitro in human lung adenocarcinoma. Pathology - Research and Practice. 2023:155038; doi: https://doi.org/10.1016/j.prp.2023.155038.
38. Li J, Zheng S, Chen B, Butte AJ, Swamidass SJ, Lu Z. A survey of current trends in computational drug repositioning. Briefings in Bioinformatics. 2015;17(1):2-12; doi: 10.1093/bib/bbv020.
39. Park K. A review of computational drug repurposing. Transl Clin Pharmacol. 2019;27(2):59-63.
40. Ko Y. Computational Drug Repositioning: Current Progress and Challenges. Applied Sciences. 2020;10(15):5076.
41. Teo ZL, Savas P, Loi S. Gene Expression Analysis: Current Methods. In: Lakhani SR, Fox SB, editors. Molecular Pathology in Cancer Research. New York, NY: Springer New York; 2016. p. 107-36.
42. Sabe VT, Ntombela T, Jhamba LA, Maguire GEM, Govender T, Naicker T, et al. Current trends in computer aided drug design and a highlight of drugs discovered via computational techniques: A review. European Journal of Medicinal Chemistry. 2021;224:113705; doi: https://doi.org/10.1016/j.ejmech.2021.113705.
43. Yella JK, Yaddanapudi S, Wang Y, Jegga AG. Changing Trends in Computational Drug Repositioning. Pharmaceuticals. 2018;11(2):57.
44. Kannaujiya VK, De Rubis G, Paudel KR, Manandhar B, Chellappan DK, Singh SK, et al. Anticancer activity of NFκB decoy oligonucleotide-loaded nanoparticles against human lung cancer. Journal of Drug Delivery Science and Technology. 2023:104328; doi: https://doi.org/10.1016/j.jddst.2023.104328.
45. Jun MY, Karki R, Paudel KR, Sharma BR, Adhikari D, Kim DW. Alkaloid rich fraction from Nelumbo nucifera targets VSMC proliferation and migration to suppress restenosis in balloon-injured rat carotid artery. Atherosclerosis. 2016;248:179-89; doi: 10.1016/j.atherosclerosis.2016.03.020.
46. Paudel KR, Kim DW. Microparticles-Mediated Vascular Inflammation and its Amelioration by Antioxidant Activity of Baicalin. Antioxidants (Basel). 2020;9(9); doi: 10.3390/antiox9090890.

47. Paudel KR, Rajput R, De Rubis G, Raju Allam VSR, Williams KA, Singh SK, et al. In vitro anti-cancer activity of a polyherbal preparation, VEDICINALS®9, against A549 human lung adenocarcinoma cells. Pathol Res Pract. 2023;250:154832; doi: 10.1016/j.prp.2023.154832.
48. Paudel KR, Karki R, Kim D-W. Cepharanthine inhibits in vitro VSMC proliferation and migration and vascular inflammatory responses mediated by RAW264. 7. Toxicology in vitro. 2016;34:16-25.
49. Lee HH, Paudel KR, Kim DW. Terminalia chebula Fructus Inhibits Migration and Proliferation of Vascular Smooth Muscle Cells and Production of Inflammatory Mediators in RAW 264.7. Evid Based Complement Alternat Med. 2015;2015:502182; doi: 10.1155/2015/502182.
50. Paudel KR, Wadhwa R, Tew XN, Lau NJX, Madheswaran T, Panneerselvam J, et al. Rutin loaded liquid crystalline nanoparticles inhibit non-small cell lung cancer proliferation and migration in vitro. Life Sci. 2021;276:119436; doi: 10.1016/j.lfs.2021.119436.
51. De Rubis G, Paudel KR, Manandhar B, Singh SK, Gupta G, Malik R, et al. Agarwood Oil Nanoemulsion Attenuates Cigarette Smoke-Induced Inflammation and Oxidative Stress Markers in BCi-NS1.1 Airway Epithelial Cells. Nutrients. 2023;15(4); doi: 10.3390/nu15041019.
52. Wirianto M, Yang J, Kim E, Gao S, Paudel KR, Choi JM, et al. The GSK-3beta-FBXL21 Axis Contributes to Circadian TCAP Degradation and Skeletal Muscle Function. Cell Rep. 2020;32(11):108140; doi: 10.1016/j.celrep.2020.108140.
53. Wickham H. ggplot2. WIREs Computational Statistics. 2011;3(2):180-5; doi: https://doi.org/10.1002/wics.147.
54. Shannon P, Markiel A, Ozier O, Baliga NS, Wang JT, Ramage D, et al. Cytoscape: a software environment for integrated models of biomolecular interaction networks. Genome Res. 2003;13(11):2498-504; doi: 10.1101/gr.1239303.
55. Doncheva NT, Assenov Y, Domingues FS, Albrecht M. Topological analysis and interactive visualization of biological networks and protein structures. Nat Protoc. 2012;7(4):670-85; doi: 10.1038/nprot.2012.004.
56. Chin CH, Chen SH, Wu HH, Ho CW, Ko MT, Lin CY. cytoHubba: identifying hub objects and sub-networks from complex interactome. BMC Syst Biol. 2014;8 Suppl 4(Suppl 4):S11; doi: 10.1186/1752-0509-8-s4-s11.
57. Brandes U. A faster algorithm for betweenness centrality*. The Journal of Mathematical Sociology. 2001;25(2):163-77; doi: 10.1080/0022250X.2001.9990249.
58. Khan MM, Serajuddin M, Malik MZ. Identification of microRNA and gene interactions through bioinformatic integrative analysis for revealing candidate signatures in prostate cancer. Gene Reports. 2022;27:101607; doi: https://doi.org/10.1016/j.genrep.2022.101607.
59. Lalwani AK, Krishnan K, Bagabir SA, Alkhanani MF, Almalki AH, Haque S, et al. Network Theoretical Approach to Explore Factors Affecting Signal Propagation and Stability in Dementia's Protein-Protein Interaction Network. Biomolecules. 2022;12(3); doi: 10.3390/biom12030451.
60. Singh SS, Haobijam D, Malik MZ, Ishrat R, Singh RKB. Fractal rules in brain networks: Signatures of self-organization. Journal of Theoretical Biology. 2018;437:58-66; doi: https://doi.org/10.1016/j.jtbi.2017.09.014.
61. Chirom K, Malik MZ, Mangangcha IR, Somvanshi P, Singh RKB. Network medicine in ovarian cancer: topological properties to drug discovery. Brief Bioinform. 2022;23(3); doi: 10.1093/bib/bbac085.

62. Sharma SK, Haobijam D, Singh SS, Malik MZ, Brojen Singh RK. Neuronal communication: Stochastic neuron dynamics and multi-synchrony states. AEU - International Journal of Electronics and Communications. 2019;100:75-85; doi: https://doi.org/10.1016/j.aeue.2019.01.006.
63. Verma RN, Malik MZ, Singh GP, Subbarao N. Identification of key proteins in host–pathogen interactions between Mycobacterium tuberculosis and Homo sapiens: A systematic network theoretical approach. Healthcare Analytics. 2022;2:100052.
64. Iqbal S, Malik MZ, Pal D. Network-based identification of miRNAs and transcription factors and in silico drug screening targeting δ-secretase involved in Alzheimer's disease. Heliyon. 2021;7(12).
65. Laskowski RA, Jabłońska J, Pravda L, Vařeková RS, Thornton JM. PDBsum: Structural summaries of PDB entries. Protein Sci. 2018;27(1):129-34; doi: 10.1002/pro.3289.
66. Friesner RA, Banks JL, Murphy RB, Halgren TA, Klicic JJ, Mainz DT, et al. Glide: A New Approach for Rapid, Accurate Docking and Scoring. 1. Method and Assessment of Docking Accuracy. Journal of Medicinal Chemistry. 2004;47(7):1739-49; doi: 10.1021/jm0306430.
67. Chaturvedi M, Mishra M, Pandey A, Gupta J, Pandey J, Gupta S, et al. Oxidative products of curcumin rather than curcumin bind to Helicobacter Pylori virulence factor VacA and are required to inhibit Its vacuolation activity. Molecules. 2022;27(19):6727.
68. Pronk S, Páll S, Schulz R, Larsson P, Bjelkmar P, Apostolov R, et al. GROMACS 4.5: a high-throughput and highly parallel open source molecular simulation toolkit. Bioinformatics. 2013;29(7):845-54; doi: 10.1093/bioinformatics/btt055.
69. Kagami L, Wilter A, Diaz A, Vranken W. The ACPYPE web server for small-molecule MD topology generation. Bioinformatics. 2023;39(6); doi: 10.1093/bioinformatics/btad350.
70. Deeba F, Malik MZ, Naqvi IH, Haider MSH, Shafat Z, Sinha P, et al. Potential entry inhibitors of the envelope protein (E2) of Chikungunya virus: in silico structural modeling, docking and molecular dynamic studies. Virusdisease. 2017;28(1):39-49; doi: 10.1007/s13337-016-0356-2.
71. Mishra CB, Pandey P, Sharma RD, Malik MZ, Mongre RK, Lynn AM, et al. Identifying the natural polyphenol catechin as a multi-targeted agent against SARS-CoV-2 for the plausible therapy of COVID-19: an integrated computational approach. Brief Bioinform. 2021;22(2):1346-60; doi: 10.1093/bib/bbaa378.
72. Rudrapal M, Paudel KR, Pangeni R. Editorial: Drug repurposing and polypharmacology: A synergistic approach in multi-target based drug discovery. Front Pharmacol. 2022;13:1101007; doi: 10.3389/fphar.2022.1101007.
73. Pushpakom S, Iorio F, Eyers PA, Escott KJ, Hopper S, Wells A, et al. Drug repurposing: progress, challenges and recommendations. Nat Rev Drug Discov. 2019;18(1):41-58; doi: 10.1038/nrd.2018.168.
74. Ganaie IA, Malik MZ, Mangangcha IR, Jain SK, Wajid S. Identification of a survival associated gene trio in chemical induced breast cancer. Biochimie. 2023;208:170-9.
75. Ganaie IA, Malik MZ, Naqvi SH, Jain SK, Wajid S. Differential levels of Alpha-1-inhibitor III, Immunoglobulin heavy chain variable region, and Hypertrophied skeletal muscle protein GTF3 in rat mammary tumorigenesis. Biochimie. 2020;174:57-68.
76. Leung ELH, Luo LX, Liu ZQ, Wong VKW, Lu LL, Xie Y, et al. Inhibition of KRAS-dependent lung cancer cell growth by deltarasin: blockage of autophagy increases its cytotoxicity. Cell Death Dis. 2018;9(2):216; doi: 10.1038/s41419-017-0065-9.

77. Sanchez-Torres JM, Viteri S, Molina MA, Rosell R. BRAF mutant non-small cell lung cancer and treatment with BRAF inhibitors. Transl Lung Cancer Res. 2013;2(3):244-50; doi: 10.3978/j.issn.2218-6751.2013.04.01.
78. Kurppa KJ, Denessiouk K, Johnson MS, Elenius K. Activating ERBB4 mutations in non-small cell lung cancer. Oncogene. 2016;35(10):1283-91; doi: 10.1038/onc.2015.185.
79. Zhang H, Zhang L, Zhou D, Li H, Xu Y. ErbB4 mediates amyloid beta-induced neurotoxicity through JNK/tau pathway activation: Implications for Alzheimer's disease. J Comp Neurol. 2021;529(15):3497-512; doi: 10.1002/cne.25207.
80. Hassan AH, Prochasson P, Neely KE, Galasinski SC, Chandy M, Carrozza MJ, et al. Function and selectivity of bromodomains in anchoring chromatin-modifying complexes to promoter nucleosomes. Cell. 2002;111(3):369-79; doi: 10.1016/s0092-8674(02)01005-x.
81. Barh D, Tiwari S, Jain N, Ali A, Santos AR, Misra AN, et al. In silico subtractive genomics for target identification in human bacterial pathogens. Drug Development Research. 2011;72(2):162-77; doi: https://doi.org/10.1002/ddr.20413.
82. Lakshmi P, Ramyachitra D. An Improved Genetic with Particle Swarm Optimization Algorithm Based on Ensemble Classification to Predict Protein–Protein Interaction. Wirel Pers Commun. 2020;113(4):1851–70; doi: 10.1007/s11277-020-07296-0.

The authors of the manuscript “Computational and Biological Approaches in Repurposing Ribavirin for Lung Cancer Treatment: Unveiling Antitumorigenic Strategies”, submitted to the journal “Life Sciences”, have no conflict of interest to declare.

Supplementary materials and methods

1.1. Cell culture and treatment with Ribavirin - H460 Cells

Human large cell lung cancer (NCI-H460, HTB177, ATCC) was cultured similarly to the A549 cell line mentioned in material and methods section 2.1. Ribavirin (Sigma-Merck, Australia) was dissolved at a stock concentration of 80 mM in sterile phosphate-buffered saline (PBS, Sigma-Merck, Australia), and diluted to the final concentration with complete DMEM.

1.2. Cell proliferation assay – MTT – H460 Cells

Cell proliferation assay was conducted similarly to the procedure mentioned in section 2.1 Cell proliferation assay - MTT

1.3. Cell migration assay – wound healing assay – H460 Cells

Cell migration assay was conducted similarly to the procedure mentioned in section 2.2 Cell migration assay – wound healing assay

Supplementary results

S1. Antiproliferative activity of ribavirin on H460 cells

As shown in supplementary figure S1, ribavirin at concentrations of 25 and 50 μM significantly inhibited the proliferation of H460 cells by 18% and 41% respectively.

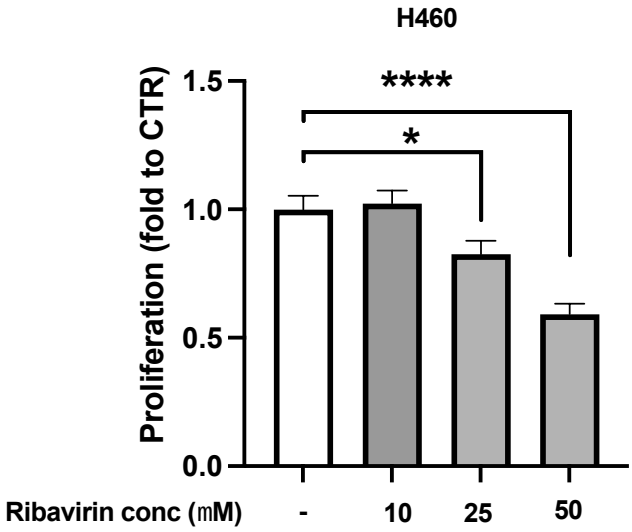

Figure S1. Assessment of the antiproliferative activity of ribavirin on H460 cells

An MTT assay was performed to test the antiproliferative activity of ribavirin on A460 cells. Statistical analysis was done with One-way ANOVA test, n=3, ****:$p<0.0001$, *:$p<0.05$ versus CTR (control cells without ribavirin treatment)

S2. Anti-migratory activity of ribavirin on H460 cells

As shown in supplementary figure S2A and S2B, ribavirin at a concentration of 25 μM significantly inhibited the migration (in terms of % wound closure) of H460 cells by 27.8% and 31.7% at 24 and 48 hours, respectively. Figure S2c shows representative figures of the wound healing assay.

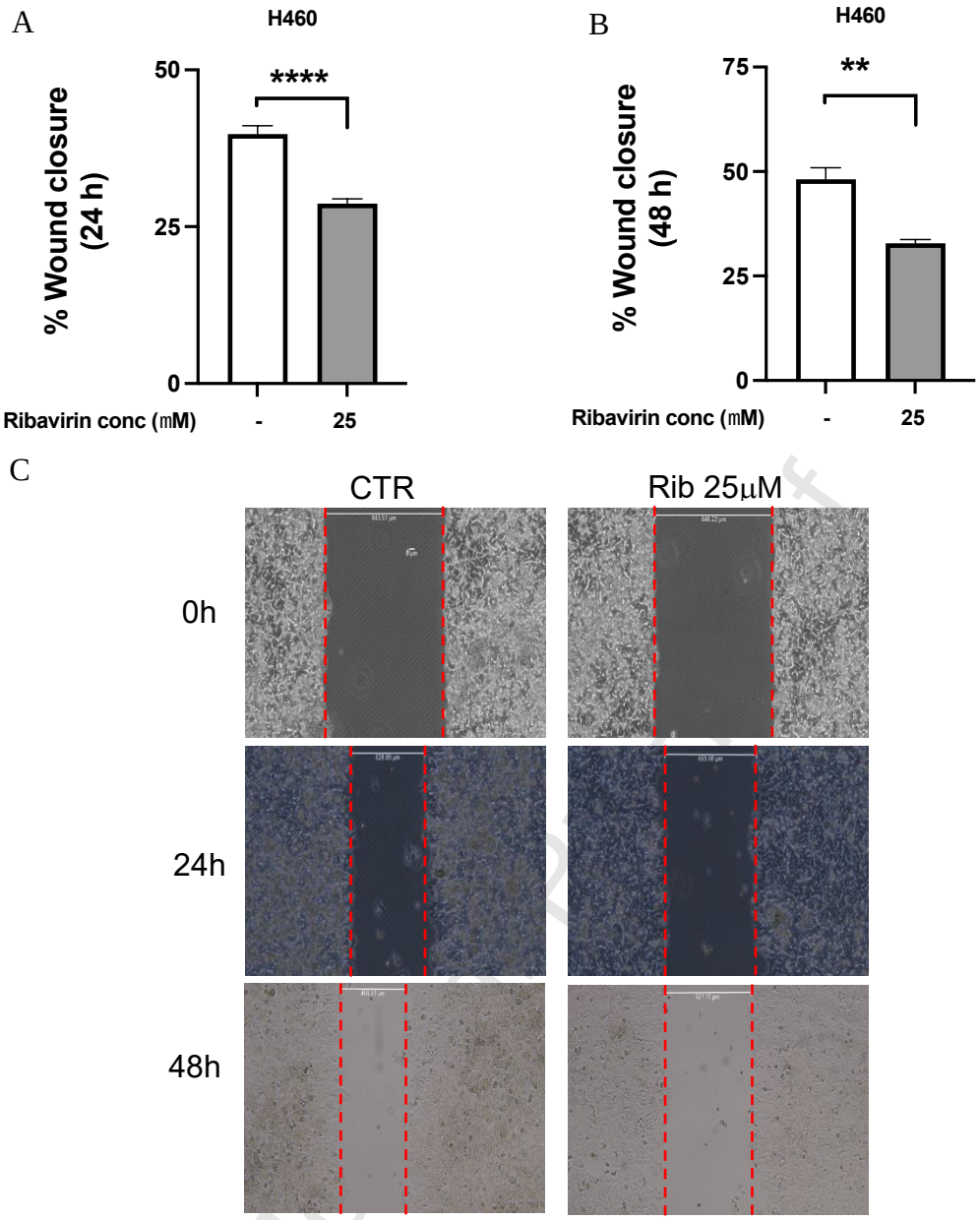

Figure S2 – Assessment of the anti-migratory activity of ribavirin on H460 cells – wound healing assay. A wound healing assay was performed to test the anti-migratory activity of 25µM of ribavirin on H460 cells. Upon scratching a confluent monolayer of H460 cells in a 6-well plate, cells were treated with 25 µM ribavirin for A) 24 h and B) 48 h and microscopic images were taken at 0 h, 24 h and 48 h. C). A) and B) show the % wound closure after 24 h treatment of ribavirin. Analysis were done with unpaired Student's t-test, n=3, **: $p<0.01$, ****: $p<0.0001$.